NIT

NASA CR-165617

Aerodynamic Analysis of VTOL Inlets and Definition of a Short, Blowing-Lip Inlet

J. Syberg and A. L. Jones

Boeing Commercial Airplane Company
Seattle, Washington

Prepared for
Lewis Research Center
under contract NAS3-22369

National Aeronautics and Space Administration

1982

AERODYNAMIC ANALYSIS OF VTOL INLETS AND DEFINITION 0F A SHORT, BLOWING-LIP INLET

by
J. Syberg and A. L. Jones

TABLE OF CONTENTS

LIST OF TABLES

LIST OF FIGURES

SUMMARY

An analytical design study was conducted to define an inlet geometry that will satisfy the design requirements typical of a tilt-nacelle VTOL aircraft. The design point, i.e., the most severe design condition selected for this study is a free stream velocity of 62 m/s (120 knots), an angle of attack of 60 degrees, and an engine corrected airflow of 78 kg/s m^2 (16 lb/sec ft^2).

The analytical results indicated that, without boundary layer control, either a very long inlet or an inlet with a very high contraction ratio lip will be required to operate separation-free at the design point. The study also showed that active boundary layer control is an effective means of preventing separation and that a significant reduction in inlet size can be achieved by removing only a small amount of bleed in the throat region of the inlet. It is believed that similar effects can be obtained by using tangential blowing.

One of the objectives of the present analytical study was to apply a NASA-developed design optimization procedure towards the design of the inlet. This procedure calls for reducing the diffuser velocity ratio at the design point by shaping the lip geometry to provide a "flat rooftop" velocity distribution. A significant reduction of the diffuser velocity ratio was obtained by following this procedure, but the boundary layer analysis indicated that the flat rooftop velocity distribution on the lip does not significantly improve the inlet separation characteristics over those obtained on a conventional inlet with a typical "peaky" lip velocity distribution.

As a separate task under the present contract a short, blowing-lip inlet model was designed and fabricated for NASA. The model is designed for testing with the Lewis Research Center's 50.8 cm fan diameter simulator. The model features a blowing slot located near the hilite on the windward side of the inlet. The slot gap is adjustable to allow optimization of the boundary layer control requirements. The basic inlet model is designed to have the fan face station at the inlet throat, i.e. the inlet has no diffuser. However, two cylindrical spacers are included with the model parts to permit an evaluation of the effects of inlet length on fan performance.

1.0 INTRODUCTION

Subsonic airplane engine inlets are generally subjected to the highest angles of attack during near-runway operation. On a tilt-nacelle VTOL aircraft the propulsion pod is rotated to a vertical position during the vertical take-off and landing transitions, which greatly increases the angle of attack on the inlet. The objectives of the present study were to analytically design and optimize an inlet for a tilt-nacelle VTOL application and to evaluate the effects of active boundary layer control on the inlet design.

The flow codes used for the aerodynamic design study include a 3-D transonic potential flow program for axisymmetric inlets at angle of attack, and a 3-D boundary layer program which is coupled with the potential flow program. Reynolds numbers corresponding to those obtained in the NASA Lewis Research Center's 9- by 15-ft Low Speed Wind Tunnel on a 50.8 cm diameter inlet model were used for the viscous analysis.

The work reported here was funded by NASA Lewis Research Center under Contract NAS3-22369.

LIST OF SYMBOLS

a	Major axis of the superellipse
b	Minor axis of the superellipse
c_F	Skin friction coefficient
CR	Contraction Ratio
DMD	Diffuser Mach number distribution
DVD	Diffuser velocity distribution
m	Exponent for x/a
m_{BLEED}	Bleed mass flow
M	Mach number
M_P	Peak Mach number
M_{TH}	Throat Mach number
n	Exponent for y/b
R	Radius
R_2	Fan face radius
R_{HI}	Hilite radius
R_{TH}	Throat radius
S	Surface distance
S_H	Surface distance along external lip measured from hilite
V	Velocity
V_0	Free stream velocity
V_{MAX}/V_{DE}	Diffuser velocity ratio: maximum velocity over diffuser exit velocity
V_x	Axial velocity
WK2/A2	Corrected airflow per unit area at fan face
x	Coordinate along major axis of the superellipse
X	Inlet station measured from hilite plane
y	Coordinate along minor axis of the superellipse
α	Inlet angle of attack

2.0 AERODYNAMIC DESIGN STUDY

2.1 OBJECTIVES AND APPROACH

In the field of subsonic propulsion aerodynamics the design of engine air inlets for tilt-nacelle VTOL airplanes, figure 1, presents a particularly challenging problem. The usually conflicting requirements of high internal performance at all flight conditions on the one hand and low cruise drag on the other hand are greatly magnified as compared to conventional subsonic inlets.

During low-speed maneuvers the main function of the inlet is to supply flow with low total-pressure distortion and high total-pressure recovery to the fan. The primary source of distortion in a subsonic inlet is separation of the boundary layer. As illustrated in figure 2, separation can occur both when the inlet airflow, i.e., throat Mach number, is too high and when it is too low.

At high throat Mach numbers, local pockets of supersonic flow tend to develop on the inlet cowl. The peak Mach number in this supersonic region will increase with angle of attack and, for high angles of attack, also with forward speed. When the shock waves, or adverse pressure gradients, become sufficiently strong, the flow separates away from the cowl surface, leading to increases in distortion and reductions in recovery. Once the inlet is separated, the distortion will increase rapidly with throat Mach number, angle of attack, and forward speed. Thus, the separation boundary is usually considered to be the inlet operating limit.

Boundary layer separation in the inlet can also occur when the inlet throat Mach number is too low. This separation occurs because the ratio of the maximum velocity (usually at or near the hilite) to the diffuser exit velocity (i.e. velocity at the engine face) increases with decreasing throat Mach number. This increased velocity ratio will eventually lead to boundary layer separation (see also references 2, 3, and 4).

The flow separation points indicated in figure 2 are dependent on the cowl boundary layer development which is in turn dependent on surface length and pressure distribution (i.e. pressure gradient). The pressure gradient can be reduced by reducing the curvature (increasing the radius of curvature) of the surface in the region of the cowl lip. As illustrated in figure 3, the reduced wall curvature results in a thicker cowl lip. The thicker cowl lip reduces the adverse pressure gradient at the low-speed condition, but increases the adverse pressure gradient for the external flow at cruise thereby reducing the drag divergence Mach number.

Thus, the central problem of the inlet design is to develop contours that will provide separation free internal flow at low speed maneuvers and throttle changes, and low-drag external flow at the cruise Mach number. The former requirement calls for a thick cowl, while the latter calls for a thin cowl. It is the designer's charter to develop contours which satisfy both requirements with minimum inlet size (i.e. weight).

One of the objectives of the present analytical study was to apply a NASA-developed design optimization procedure towards the design of a VTOL inlet and compare this configuration to an existing lift/cruise fan inlet (herein referred to as the baseline inlet) which was developed by Boeing using more conventional design optimization procedures (references 3 and 4). A schematic of this inlet is shown in figure 4. This inlet is asymmetric to minimize the external dimensions. The windward side contours, which were used for the analysis of the baseline inlet, are shown in this figure. An additional objective was to design an inlet with boundary layer control and compare this configuration to the baseline inlet.

NASA OPTIMIZATION PROCEDURE

The NASA-developed optimization procedure is described in detail in reference 1. Briefly, the procedure consists of two iterative loops. The outer loop is for determination of the "design point" (i.e. the point on the operating envelope where boundary layer separation is most likely to occur) and calculation of the inlet separation boundaries (figure 2), and the inner loop is for obtaining the optimum lip and diffuser geometries. In the present study the outer loop of the procedure was deleted. Instead, the design point was to be defined from analysis of the baseline inlet (see Section 2.2).

The inner loop procedure consists of perturbing the lip and diffuser geometries until specific requirements to the lip pressure distribution and the skin friction distribution have been met. These requirements are illustrated in figures 5 and 6 (figures 8 and 9 in reference 1). According to reference 1, the "Modified Optimum" distributions are expected to provide the best overall inlet design. Constraining parameters in the lip optimization are the ratio of maximum surface velocity to the diffuser exit velocity (diffusion ratio) and the maximum surface Mach number. Empirically determined limits for these parameters are described in reference 2.

ANALYSIS TOOLS

The flow codes used for the inlet aerodynamic design study are a 3-D transonic potential flow program for axisymmetric inlets at angle of attack, and a 3-D boundary layer program which is coupled with the potential flow program. The potential flow program solves the complete potential flow equation for the flow fields about axisymmetric inlets or bodies operating at angle of attack. The free-stream Mach number must be subsonic, but the local flow about the body may be transonic.

The exact potential flow equation expressed in a cylindrical coordinate system is solved using finite differences and line relaxation. Several techniques are used to speed convergence and thus minimize the cost of a computer run. These techniques include use of coarse meshes for starting and initial relaxation, fine meshes for the final relaxation, extrapolation of residue fields when they are steady for several successive relaxation sweeps, and special θ differencing to minimize the number of θ-mesh required. Program output includes complete details of the flow field about the inlet and at the inlet surface including plots of geometry and surface Mach number at the user's request.

The boundary layer calculation method is embodied in a computer program which uses a finite difference method to solve the compressible boundary layer equations along attachment lines (lines of symmetry) of three-dimensional bodies and the three-dimensional, compressible laminar or turbulent boundary layer equations in curvilinear, orthogonal coordinates for the rest of the body surface. The numerical method is implicit with regard to the solution in the coordinate normal to the surface and the differencing in the other two coordinates adapts to the direction of the local velocity vector in a manner consistent with the zones of dependence and influence in the governing equations. The method is general in nature and can be applied in any surface-fitted orthogonal grid for which some mild restrictions on the velocity field are satisfied and for which initial conditions sufficient to determine the boundary layer solution can be satisfied.

A 2-D/axisymmetric boundary layer program was used for designing the inlet with boundary layer control. This program provides a finite-difference solution of the boundary layer equations. It computes laminar and turbulent boundary layer development on two-dimensional or axisymmetric surfaces with or without bleed and with or without heat transfer. Oblique shock/boundary layer interactions are computed using a control volume analysis. Boundary layer transition may be specified as occurring at a given location or given momentum thickness Reynolds number.

The above computer codes are all developed at Boeing and have been used extensively for a number of in-house inlet design studies.

2.2 DESIGN POINTS

The first step in the optimization procedure is to define the design point, i.e. the most severe condition within the operating envelope of the inlet. In the present study, this was accomplished by comparing test results for the baseline inlet (references 3 and 4) with the estimated operating schedule (forward speed, angle of attack, engine airflow range) for a typical tilt-nacelle VSTOL inlet, see figure 7.

The test results from reference 4 indicate that the most severe operating conditions on this envelope are points A and B. At point A, diffuser separation is more likely to occur than at any other point along the minimum airflow curve. At point B, the lip peak Mach number will be higher than at any other point along the maximum airflow curve. Thus, the design points selected for the aerodynamic design study are:

A.	free stream velocity,	V_0 = 62 m/s (120 knots)
	angle of attack,	α = 60 degrees
	engine corrected airflow,	WK2/A2 = 78 kg/s m^2 (16 lb/sec ft^2)
B.	free stream velocity,	V_0 = 39 m/s (75 knots)
	angle of attack,	α = 90 degrees
	engine corrected airflow,	WK2/A2 = 200 kg/s m^2 (41 lb/sec ft^2)

Point A applies to the low throat Mach number separation depicted in figure 2 while point B applies to the separation caused by high throat Mach numbers. The design problem, therefore, is to define an inlet geometry that provides separation-free flow at both operating points.

2.3 LIP STUDY

With the design point conditions defined, an analysis was first made to determine the velocity ratio (V_{MAX}/V_{DE} at condition A and the peak Mach number (M_P) at condition B for the baseline inlet. As shown in figure 8, the peak Mach number at condition B is significantly lower than the empirically determined peak Mach number limit of about 1.5 (reference 2), whereas the velocity ratio at condition A is somewhat higher than the empirical limit of 2.4-2.9 (reference 2). These results indicate that condition A is by far the most severe design condition for an inlet without boundary layer control. The results also suggest that it will be necessary to increase the contraction ratio and/or improve the lip shape to meet the design requirements.

As indicated in figure 5, the NASA optimization procedure calls for a lip geometry that produces a constant velocity across the surface of the lip. The hypothesis is that such a lip will reduce the overall diffuser velocity ratio, which in turn will improve the inlet separation characteristics without requiring a thicker lip.

To obtain a constant velocity profile lip, modifications were made to the baseline inlet lip by using various combinations of the exponents n and m in the superelliptical equation:

$$\left(\frac{x}{a}\right)^n + \left(\frac{y}{b}\right)^m = 1$$

The inlet contours analyzed were identical to those of the baseline inlet except for the lip region. Thus, the hilite and throat locations remained fixed while the contours between these points were varied. Some of the analytical results are illustrated in figures 9 and 10.

It is evident from figure 9 that large variations in lip Mach number distribution can be achieved by varying the superelliptical exponents. In figure 10, the Mach number distributions for a number of refined configurations are shown.

Figure 11 presents the Mach number distributions for the best "flat rooftop" lip found during the present study. This configuration (No. 16) was obtained using exponents of n=3.65 and m=1.65. Note that the near-constant velocity region extends over only 1/3 of the lip arc length as opposed to the entire lip length called for in reference 1 (see figure 5).

Studies were also conducted to determine if the flat rooftop velocity profile can be improved by varying the lip fineness ratio (a/b). Figure 12 shows the Mach number profiles for three different fineness ratios, including that of configuration 16. The shapes for the a/b = 2.0 and 2.5 lips were obtained by multiplying the axial coordinates of the configuration 16 lip by 0.887 and 1.109, respectively. For these lip shapes it appears that the fineness ratio for the configuration 16 lip is near optimum. It is believed that both the a/b = 2.0 and the a/b = 2.5 lip Mach number distributions can be flattened by individually optimizing the superelliptical exponents. However, there is no indication that this would produce a velocity profile "rooftop" which is lower and wider than that of configuration 16. Consequently, configuration 16 is considered the optimum lip in terms of producing a flat rooftop velocity distribution at the design point.

The contours of the flat rooftop lip are compared with those of the baseline in figure 13. To achieve the constant velocity profile, the curvature has been reduced in the hilite and throat regions and increased near the middle of the lip.

Figure 14 compares the Mach number distributions at design point A for the two inlets. The lip contour change has reduced the diffuser velocity ratio from 3.23 to 2.87. According to references 1 and 2, this should expand the separation-free operating range of the inlet.

Skin friction calculations made for the two inlets are presented in figure 15. These results indicate that the flat rooftop inlet actually separates upstream of the baseline inlet, thus contradicting references 1 and 2. However, an important consideration in any boundary layer analysis is the location of the transition region between laminar and turbulent flow. In the above calculations, the transition was assumed to take place right at the peak Mach number (just inside the hilite) on both inlets. As illustrated on figure 16, the flat rooftop distribution may possibly delay the transition to the point where the strong adverse pressure gradient begins. Figure 17 shows the effect of the transition criteria. Delayed transition improves the skin friction coefficient distribution such that the flat rooftop inlet now appears to be slightly better than the baseline inlet.

The preceding discussion addresses the effects of lip shape and lip fineness ratio. Another significant parameter in the design of a subsonic inlet is the lip contraction ratio, $(R_{III}/R_{TH})^2$. Since the diffuser velocity ratio of the best flat rooftop inlet (configuration 16) is higher than the average empirical limit (2.65) defined in reference 2, it will be necessary to increase the contraction ratio to meet the design requirements. However, one of the ground rules set for the present study was that the contraction ratio should not exceed that of the baseline inlet. Thus, only a cursory study of the effects of contraction ratio was conducted. The results are shown in figures 18 and 19. Using the same superelliptical exponents and fineness ratio as those of configuration 16, a lip with a contraction ratio of 2.0 was designed. As shown in figure 18, this method provided a lip with a flat rooftop Mach number distribution similar to that of configuration 16. However, the velocity ratio is still higher than the empirical limit, indicating that it will be necessary to further increase the contraction ratio. Figure 19 confirms this finding. The high contraction ratio inlet separates downstream of configuration 16 but still upstream of its throat. Since a contraction ratio of 2.0 is already unrealistically high, no further studies of the effects of contraction ratio were conducted.

2.4 DIFFUSER STUDY

Since all lip optimization attempts have failed to produce a separation-free inlet at the very severe conditions of design point A, the attention was focused on optimization of the diffuser velocity distribution. An independent study conducted by NASA had shown that, with a velocity ratio equal to 2.79, a velocity distribution exists that allows separation-free diffusion. Since the velocity ratio of configuration 16 (the flat rooftop lip) is only slightly greater than that studied by NASA (2.87 compared to 2.79), it would appear that it is possible to obtain attached flow at condition A through proper design of the diffuser.

The velocity distributions studied by NASA are shown in Figure 20. The corresponding skin friction coefficient profiles predicted by NASA are presented in figure 21. To compare NASA's

and Boeing's computer codes, the velocity distributions from figure 20 were input to a Boeing 2-D finite-difference boundary layer program (see Section 2.1). The results, which are shown in figure 22, agree well with NASA's boundary layer analysis.

Using the lip velocity distribution of configuration 16, five hypothetical velocity distributions, similar to those shown in figure 20, were then defined. These distributions are illustrated in figure 23. The results of the boundary layer analysis of these velocity distributions are shown in figure 24. All five velocity distributions induce boundary layer separation upstream of the throat and there is no indication that a successful configuration exists within the range of distributions analyzed. It appears that the slightly higher velocity ratio (2.87 as opposed to 2.79) coupled with the thicker laminar boundary layer (longer constant velocity region) are responsible for the difference between these results and those shown in figure 22.

As indicated in figure 23, the Mach number distributions of configuration 16 and DMD5 are very similar up to a distance of $S/R_2 = 0.66$. An investigation was conducted to determine if a Mach number distribution exists between DMD5 and configuration 16, see figure 25, that will meet the design requirements of design point A. The results are shown in figure 26. All DMD's caused boundary layer separation upstream of that predicted for configuration 16 (compare with figure 17).

It would appear from the above studies of various hypothetical constant-length diffuser Mach number distributions, that any diffuser that diffuses more rapidly than configuration 16 in the forward part of the diffuser will cause boundary layer separation farther upstream than configuration 16. It was concluded that a longer diffuser would be required to obtain attached flow at design point A.

Various modifications were therefore made to the Mach number distributions of configuration 16. Each DMD modification was input to the 2-D boundary layer program. Based on the calculated skin friction coefficient profile the DMD was adjusted and a new boundary layer analysis performed. This procedure was repeated until a successful DMD was found. The results are illustrated in figures 27 and 28. DMD's 17-21 cause separation upstream of the corresponding diffuser exits while DMD 22 is the first configuration that provides attached flow at design point A. These results are also illustrated in figure 29. The minimum diffuser length required to avoid separation is approximately 3.1 fan face diameters. This length is almost twice the length of the baseline inlet, see figure 30, and is considered impractical for a VSTOL application. Consequently, the final step in the design process, namely to define the diffuser geometry that provides the Mach number distribution shown in figure 30, was not performed.

2.5 BOUNDARY LAYER CONTROL STUDY

The analytical results described in Sections 2.3 and 2.4 predict that it is not possible to achieve a satisfactory inlet geometry that will meet the stringent requirement imposed on the present design. This section describes the effects of active boundary layer control on the inlet geometry when designed for the same stringent design requirements. Suction, i.e. bleed, is used as the method of controlling the boundary layer development.

The viscous analysis of inlets without boundary layer control (BLC), Section 2.3, indicated that only a small improvement is achieved by shaping the lip to obtain a flat rooftop velocity distribution, and that the improvement will be realized only if transition occurs near the downstream end of the rooftop. Consequently, the baseline inlet was used also as a baseline for the BLC study.

The baseline inlet and several derivatives thereof were analyzed to determine the minimum amount of bleed mass flow required to prevent boundary layer separation at condition A. The baseline derivatives were obtained by scaling down the baseline inlet along vectors originating at point F in figure 31. Scale factors were used that provided equal increments in the contraction ratio, i.e. CR = 1.75, 1.70, 1.65, ..., 1.30.

To determine the minimum amount of bleed mass flow at condition A, two flow codes were used, namely a 3-D transonic potential flow program and a 2-D boundary layer program with built-in bleed capability. These computer programs are described in Section 2.1.

The aerodynamic design analysis consisted of four steps. The first step was to determine the peak Mach numbers using the potential flow code at condition B (see Section 2.2) for each contraction ratio. The peak Mach numbers are presented in figure 32. Figure 32 shows that the contraction ratio should be greater than 1.40 to satisfy the peak Mach number limit of 1.5 (reference 2).

The second step was to determine the windward plane Mach number distributions at condition A for each contraction ratio (see figure 33). These distributions were used as inputs to the boundary layer program for calculation of the boundary layer properties.

The third step consisted of determining the location and dimensions of the bleed region. The point of separation without boundary layer control was determined for each inlet using the boundary layer program. A bleed region was then located slightly upstream of the separation point for each contraction ratio. For simplicity, all of the bleed regions analyzed were rectangular (see figure 34) with the same axial length and the same circumferential extent ($\pm 45^0$).

The fourth step of the analysis procedure was to determine, for each contraction ratio, the minimum bleed mass flow required to obtain attached flow at condition A. Bleed mass flows were input into the boundary layer program and the skin friction distributions were compared. This process was repeated until the bleed mass flow was minimized for each contraction ratio. Figure 35 illustrates this procedure for the CR = 1.55 configuration. The figure indicates that

the minimum bleed mass flow for this case is between 0.107 kg/s and 0.113 kg/s. Figure 36 summarizes the results of the boundary layer control study. It is evident from this figure that the minimum bleed mass flows are relatively low (less than 0.75% of the inlet mass flow) and that the increase in boundary layer bleed with decreasing contraction ratio is surprisingly small.

As described above, the present BLC study was conducted by determining the effects of boundary layer bleed on the inlet separation characteristics. It is believed that similar effects can be achieved by blowing a sufficient amount of high-pressure air tangentially into the boundary layer. Unfortunately, a BLC blowing system cannot be accurately designed with any of the computer codes available for this program and will probably require extensive experimental development work.

2.6 CONCLUDING REMARKS

The analytical studies indicated that, without boundary layer control, either a very long inlet or an inlet with a very high contraction ratio lip will be required to meet the design requirements imposed on the present VTOL design. A thorough optimization of the inlet geometry, using the NASA-developed optimization procedure, therefore was not possible.

As suggested by NASA, the diffuser velocity ratio at a given condition can be reduced by shaping the lip geometry to provide a flat rooftop velocity distribution. Analyses of the boundary layer development indicate, however, that the flat rooftop lip does not significantly improve the inlet separation characteristics over those obtained on a conventional inlet with a typical "peaky" lip velocity distribution.

The study also showed that active boundary layer control is an effective means of preventing separation at low throat Mach numbers (i.e. design point A) and that a significant reduction in inlet size can be achieved by removing only a small amount of bleed in the throat region of the inlet. It is believed that similar effects can be obtained by using BLC blowing.

3.0 DEFINITION OF A SHORT, BLOWING-LIP INLET

As a separate task under the present contract a short, blowing-lip inlet model was designed and fabricated for NASA. The model is designed for testing with the NASA Lewis 50.8 cm fan simulator. This section describes the inlet model, the aerodynamic contours and the model instrumentation. A test plan for the wind tunnel test is also provided. The model design is defined in Boeing drawings G5735-1 through -6.

3.1 INLET GEOMETRY

A schematic of the blowing lip inlet model is presented in figure 37. The model consists of a hollow lip with an adjustable slot near the hilite on the windward side of the inlet. A connector for the high-pressure airflow supply pipe is provided on the leeward side of the external lip. The model structure is designed for a plenum pressure equal to 1.5 times the atmospheric pressure. Included with the model are a 5.08 cm and a 10.16 cm long spacer ring. These spacer rings will allow testing the lip with extensions of 5.08 cm, 10.16 cm, and 15.24 cm.

The contraction ratio of the internal lip is 1.30. As shown in figure 38, the shape of the lip is elliptical ($n = m = 2$) with a fineness ratio $a/b = 2.0$. The external lip is also elliptical with $a/b = 5.0$ and $R_H/R_{MAX} = 0.864$. Only the forward 50 mm of the external lip contours are simulated on the model.

The circumferential extent of the slot is 120 degrees, while the plenum inside the lip extends over the full circumference. The slot is located approximately 9 mm inside the hilite. The outer lip can be translated to vary the slot gap up to a maximum width of 1.5 mm. Detail contours of the slot region are provided in figure 39.

3.2 INSTRUMENTATION

The instrumentation provided with the model consists of 94 static pressure taps, three plenum pressures, and two thermocouples. The exact locations of this instrumentation are defined in figure 40.

3.3 PRELIMINARY TEST PLAN

The main objective of the program is to evaluate the feasibility of using a blowing slot near the hilite of the inlet lip to delay boundary layer separation in a short inlet during high angles of attack. The effects of varying the massflow and velocity through the blowing slot will be evaluated both by changing the total pressure of the jet and by changing the slot dimensions. The program also offers an opportunity to examine the effects of various degrees of flow non-uniformity at the fan face on the fan operating characteristics. The test plan suggested by Boeing is structured to accomplish these objectives within the two-week test period allowed for this program.

TEST SEQUENCE NO. 1

This series of tests is aimed at obtaining a preliminary definition of the effects of blowing and at gaining some experience with the general operation of the boundary layer control system and with detection of the onset of separation.

The test matrix is shown in Table 1.

Table 1. Test Matrix for Sequence No. 1

Slot Gap G (mm)	Tunnel Speed V_o (m/s)	Inlet Corr. Flow WKA (kg/s m^2)	Plenum Pressure P_{PL}/P_{TO}
1.0	39 and 62	80	1.00
			1.25
			1.50
		120	1.00
			1.25
			1.50
		160	1.00
			1.25
			1.50
		200	1.00
			1.25
			1.50

Test Procedure:

(1) Set V_o, WKA, and P_{PL}/P_{TO} at $\alpha = 0^0$.

(2) Increase α to separation, recording data at every 10 degrees as well as just before and just after separation.

TEST SEQUENCE NO. 2

This test series will provide detailed information on the effects of slot gap setting, plenum pressure, and inlet length at operating conditions typical of a tilt-nacelle VTOL aircraft inlet.

The test matrix is illustrated in Table 2.

Table 2. Test Matrix for Sequence No. 2

Spacer Length L (cm)	Slot Gap G (mm)	Tunnel Speed V_0 (m/s)	Angle of Attack α (degrees)	Inlet Corr. Flow WKA (kg/s m^2)
		62	60	80 120 160 200
0	0.5, 1.0, and 1.5	39	90	80 120 160 200
		21	120	80 120 160 200
5, 10, and 15	One setting, to be determined after testing without spacers	62	60	80 120 160 200
		39	90	80 120 160 200
		21	120	80 120 160 200

Test Procedure:

(1) Set V_0, α, and WKA

(2) Vary P_{PL}/P_{TO} from maximum (1.5) to minimum (no flow), recording approximately six equally spaced data points as well as points just before and just after separation where applicable.

3.4 CONCLUDING REMARKS

A 50.8 cm inlet model has been built for testing with the NASA Lewis fan simulator. The model features a blowing slot located near the hilite on the windward side of the inlet. The slot gap is adjustable to allow optimization of the boundary layer control requirement.

The basic inlet model is designed to have the fan face station at the inlet throat, i.e. the inlet has no diffuser. However, two cylindrical spacers are included with the model parts to permit an evaluation of the effects of inlet length on fan performance.

A test plan which considers the above model variables has been prepared. This plan is structured to accomplish the test objectives within a two-week test period.

REFERENCES

1. R. W. Luidens, N. O. Stockman, and J. H. Diedrich, "An Approach to Optimum Subsonic Inlet Design," NASA TM 79051, March 1979.

2. M. A. Boles and N. O. Stockman, "Use of Experimental Separation Limits in the Theoretical Design of V/STOL Inlets," NASA TM 73709, July 1977.

3. J. L. Koncsek and R. J. Shaw, "Operating Characteristics of an Inlet Model Tested with a 0.5 Meter Powered Fan at High Angles of Attack," NASA CR-135270, September 1977.

4. J. Syberg, "Low Speed Test of a High-Bypass Ratio Propulsion System with an Asymmetric Inlet Designed for a Tilt-Nacelle V/STOL Airplane," NASA CR-152072, January 1978.

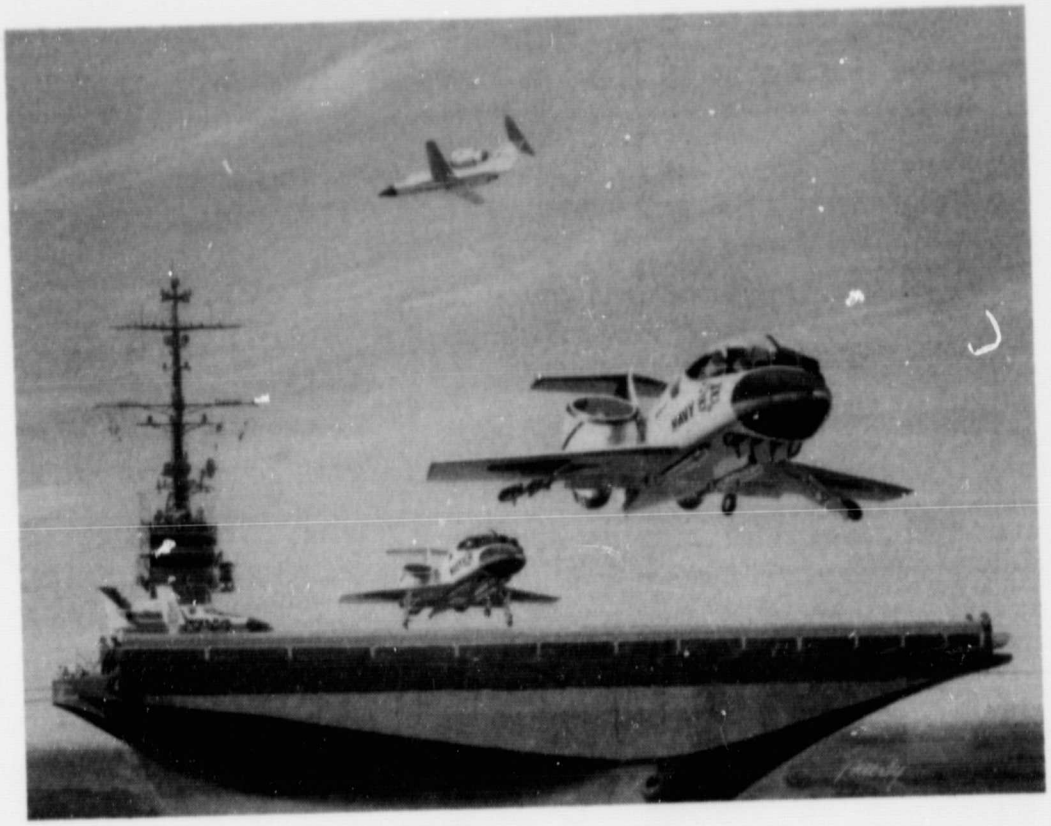

Figure 1. Tilt-Nacelle Lift-Cruise Fan Concept

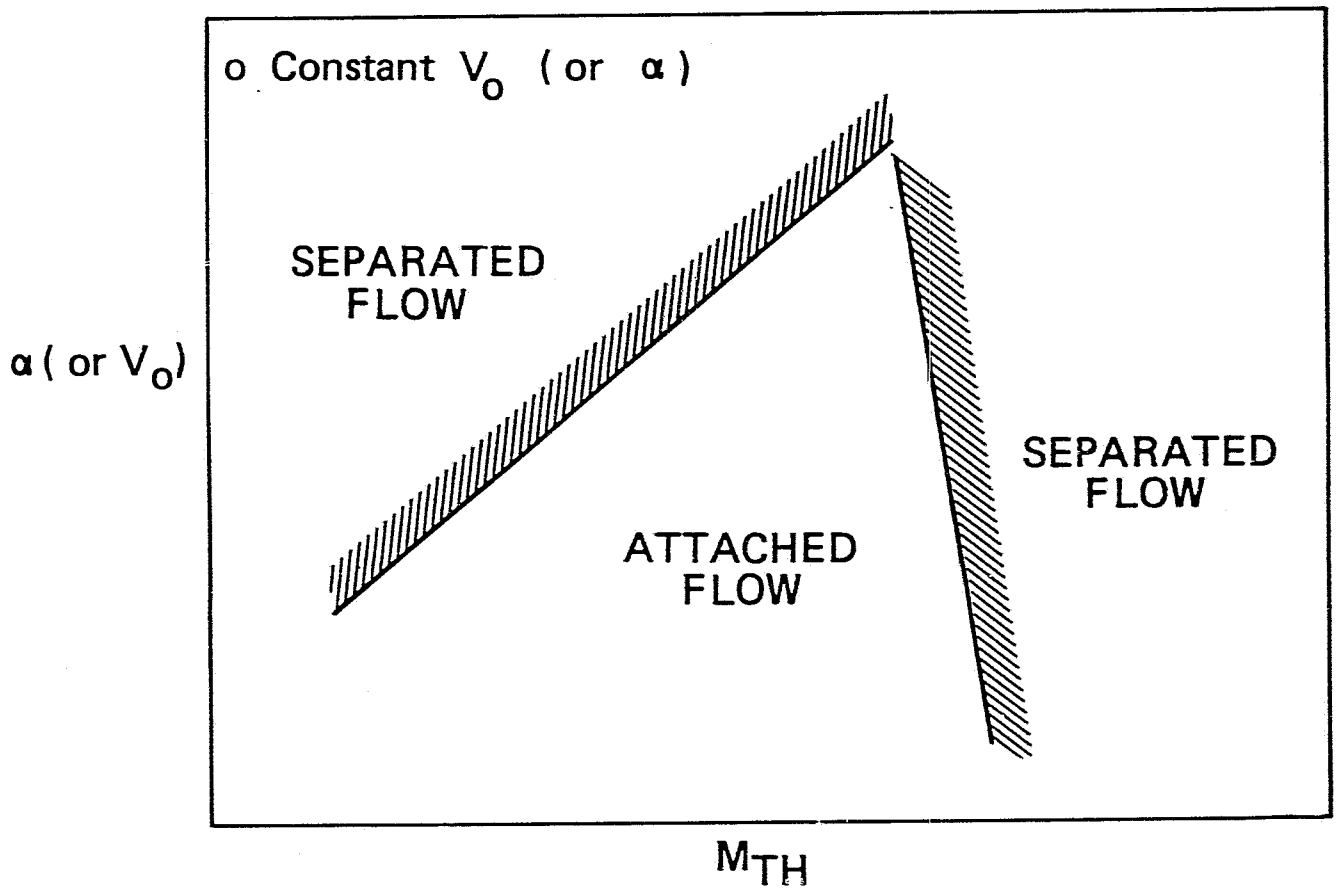

Figure 2. Inlet Separation Boundaries

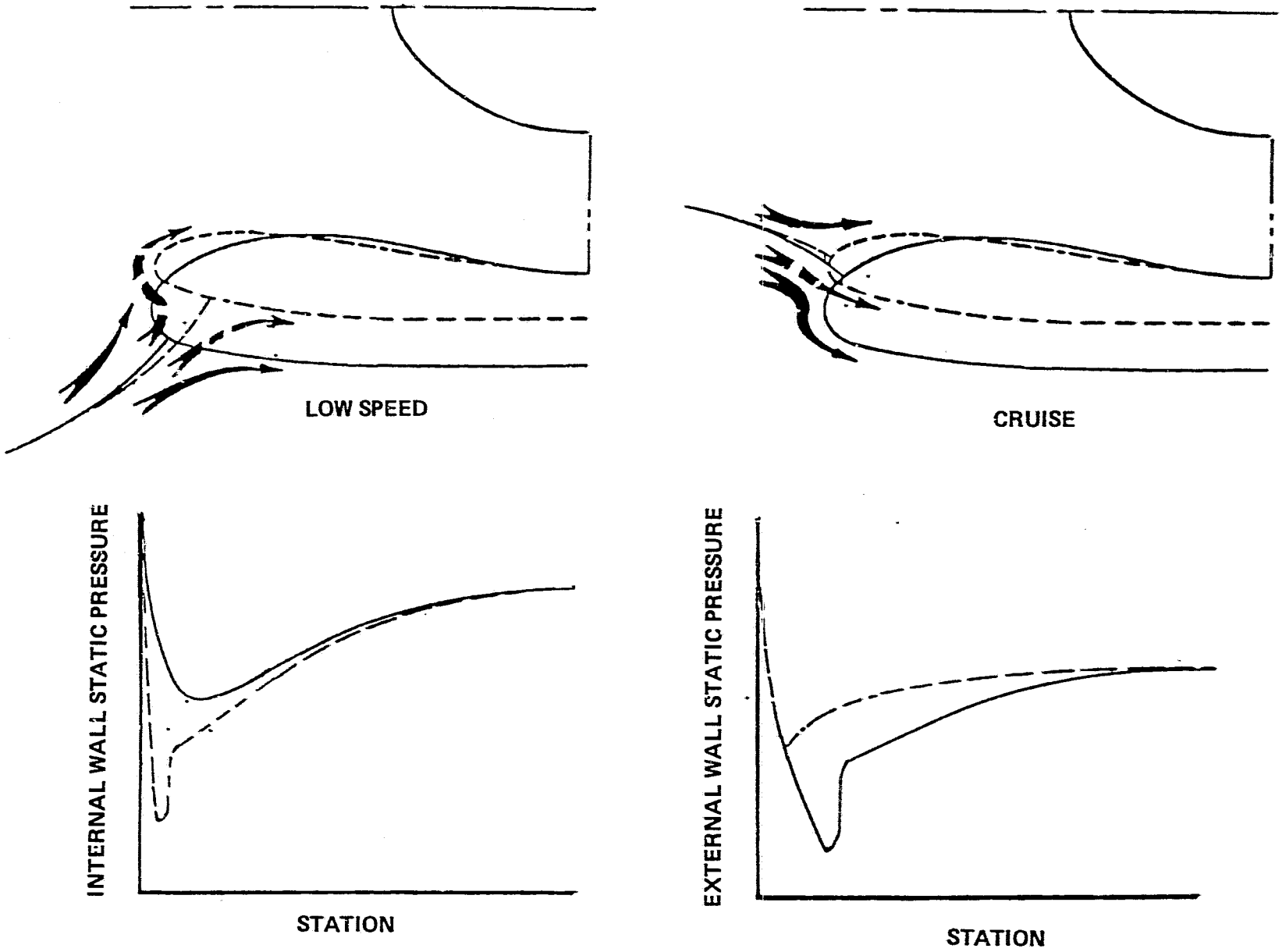

Figure 3. Effects of Cowl Wall Curvature on Inlet Lip Pressure Distribution

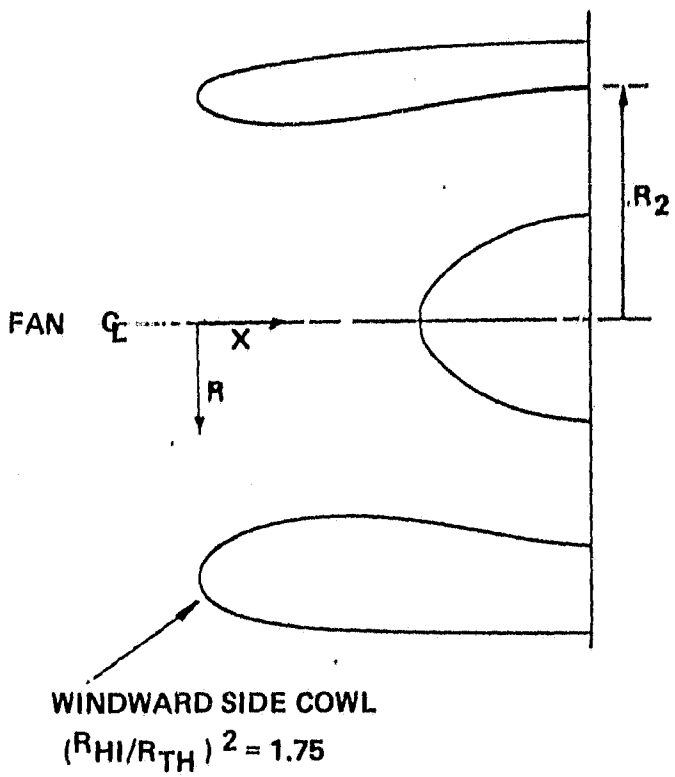

WINDWARD SIDE COWL CONTOURS

X/R_2	R/R_2	X/R_2	R/R_2
1.146	1.344	.223	.917
1.072	1.344	.280	.897
.959	1.342	.336	.882
.846	1.339	.393	.870
.784	1.336	.450	.861
.733	1.334	.506	.856
.676	1.330	.563	.853
.620	1.327	.620	.853
.563	1.322	.676	.855
.506	1.318	.733	.859
.450	1.312	.784	.866
.393	1.306	.846	.874
.336	1.299	.959	.894
.280	1.290	1.072	.917
.223	1.283	1.146	.933
.167	1.272	1.164	.936
.138	1.265	1.273	.959
.110	1.255	1.382	.978
.082	1.244	1.491	.992
.054	1.228	1.600	1.000
.035	1.212	1.637	1.000
.016	1.180		
.008	1.173		
.003	1.155		
0.000	1.127		
0.003	1.107		
.008	1.088		
.016	1.071		
.035	1.043		
.054	1.021		
.082	.995		
.110	.975		
.138	.967		
.167	.942		

Figure 4. Baseline Inlet

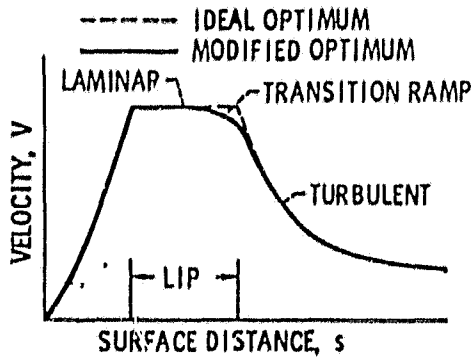

Figure 5. Optimum Lip Velocity Distribution

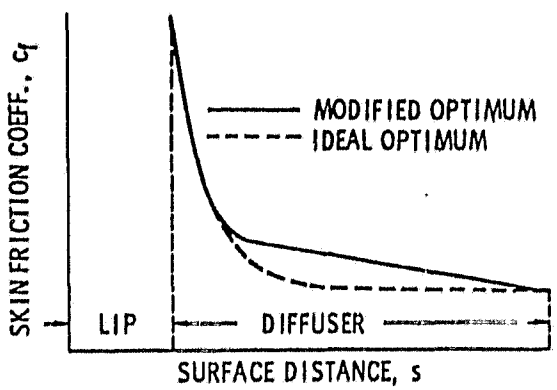

Figure 6. Optimum Diffuser Skin Friction Coefficient Distribution

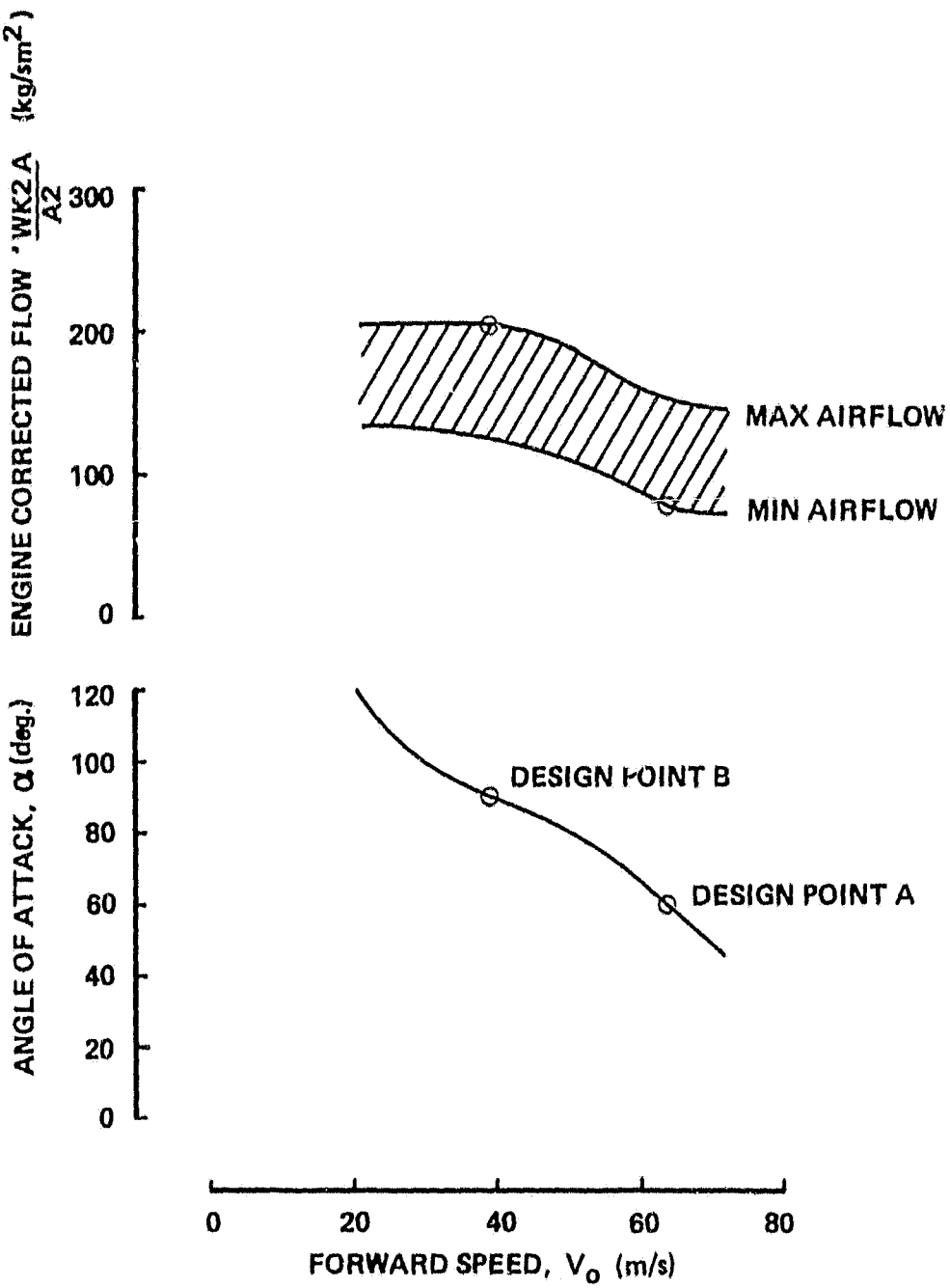

Figure 7. Estimated Design Envelope for Typical Tilt-Nacelle VSTOL Inlet

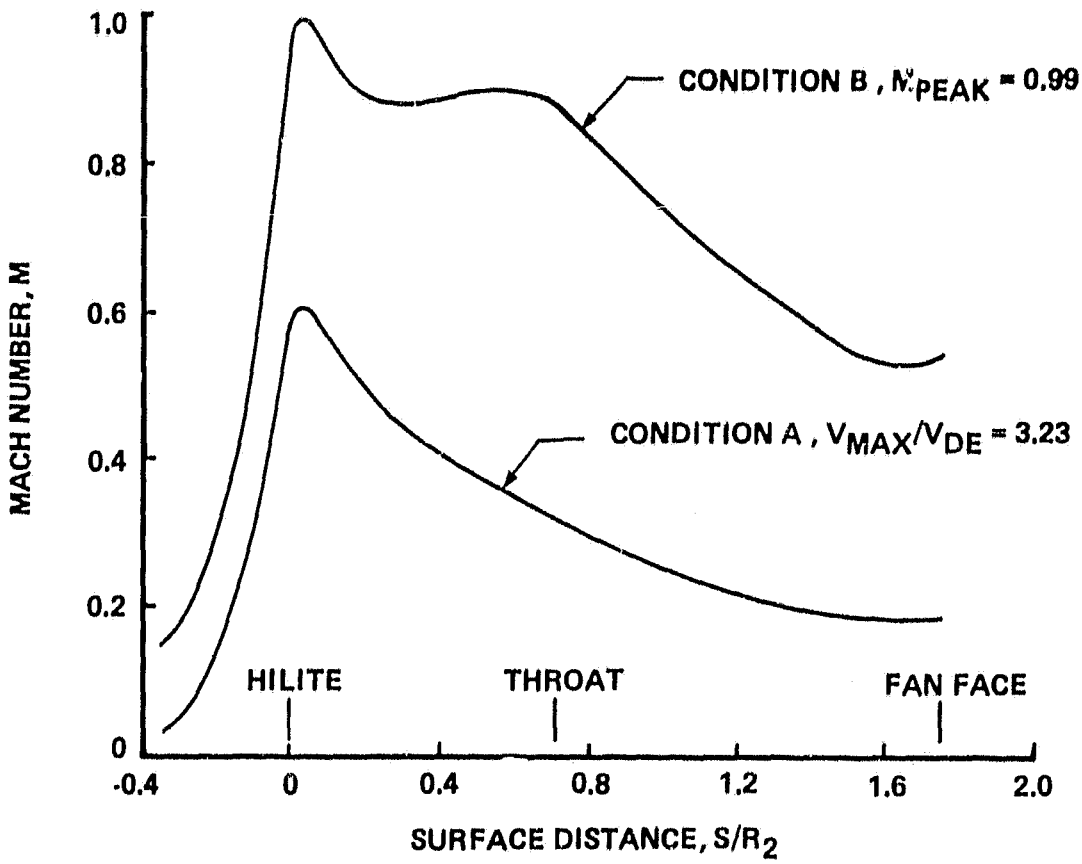

Figure 8. Mach Number Distributions at Conditions A and B for Baseline Inlet

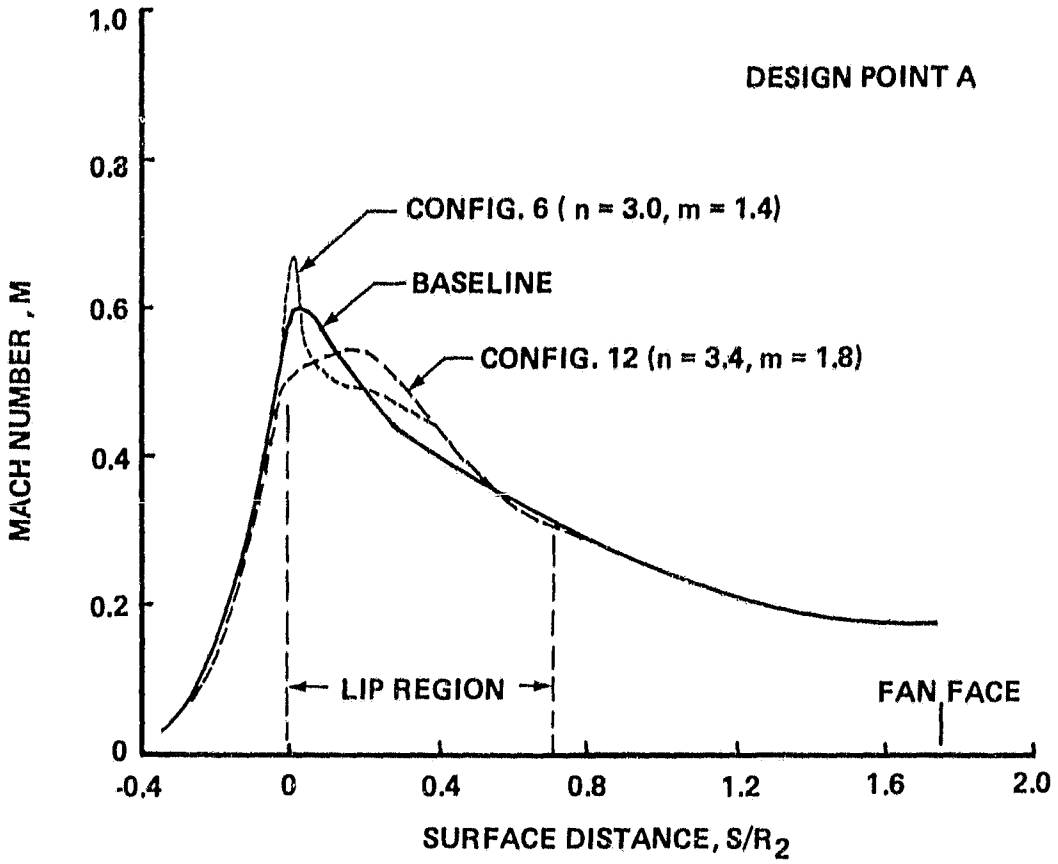

Figure 9. Windward Side Mach Number Distributions for Various Superelliptical Lip Shapes and Baseline Inlet

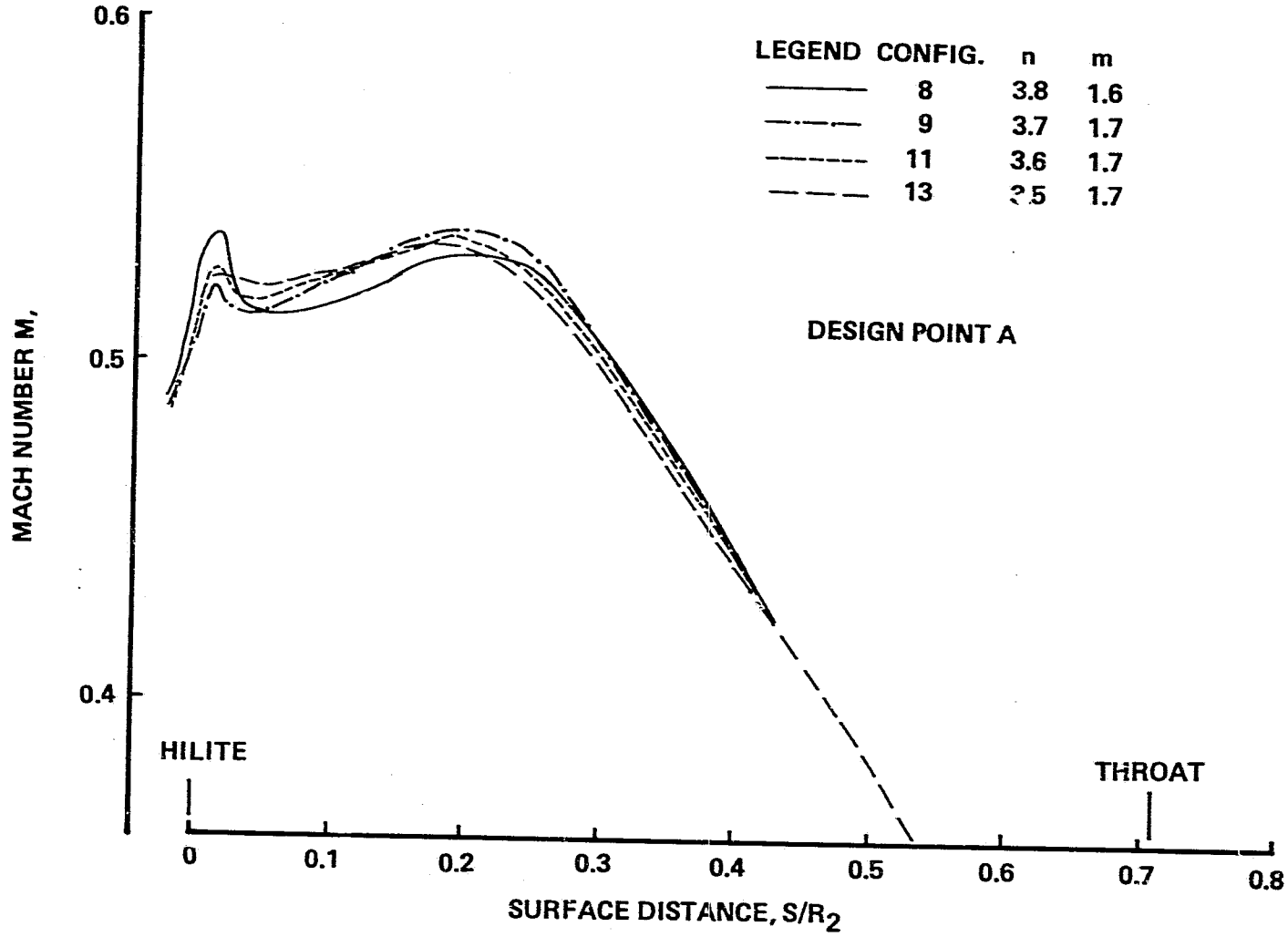

Figure 10. Lip Mach Number Distributions for Refined Configurations

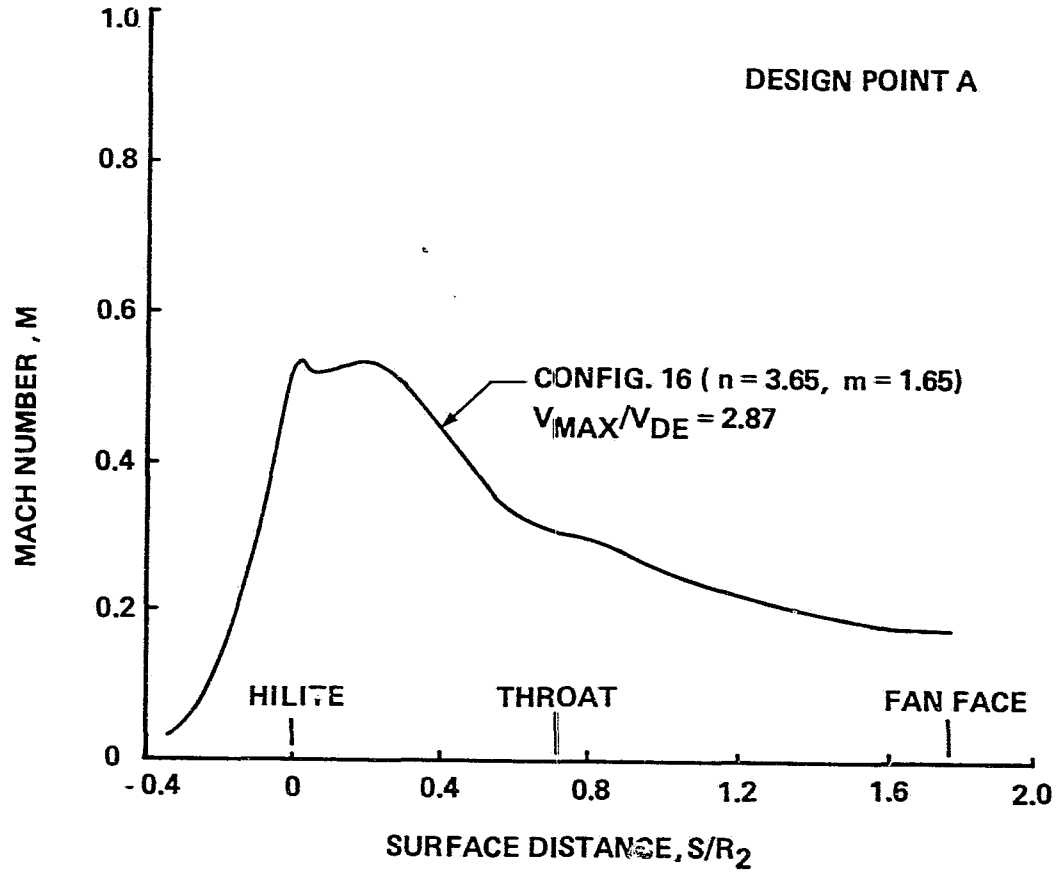

Figure 11. Best "Flat Rooftop" Lip Mach Number Distribution

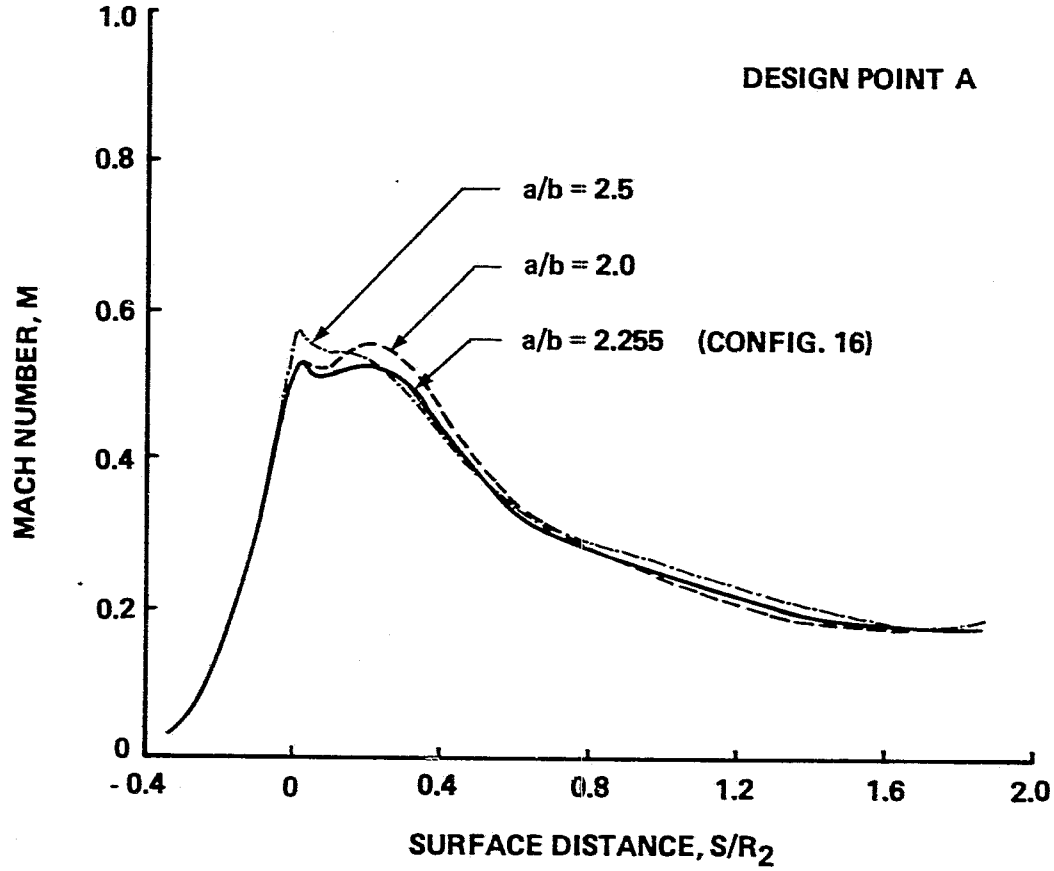

Figure 12. Effect of Lip Fineness Ratio on Mach Number Distribution

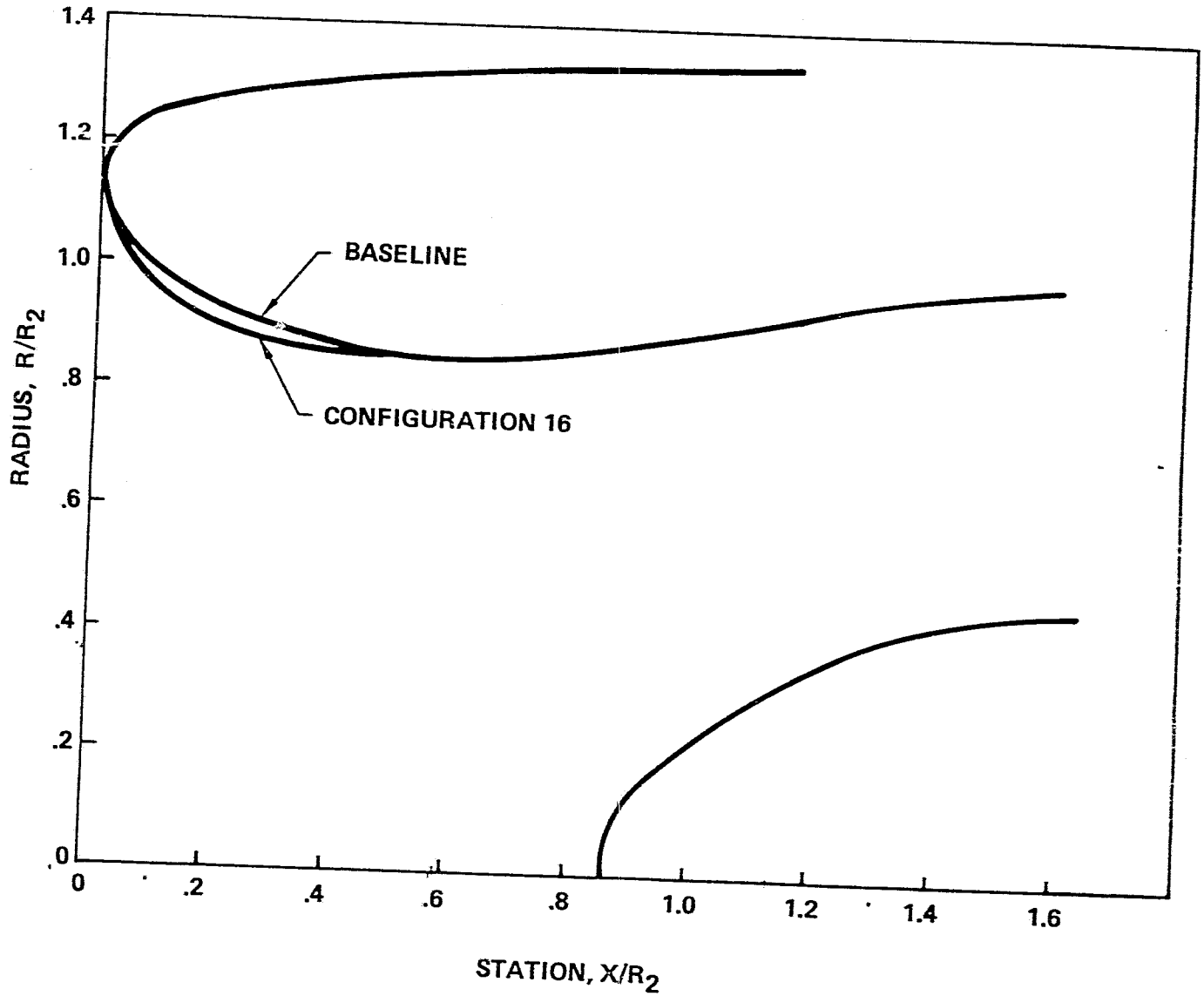

Figure 13. "Flat Rooftop" Lip and Baseline Lip Geometries

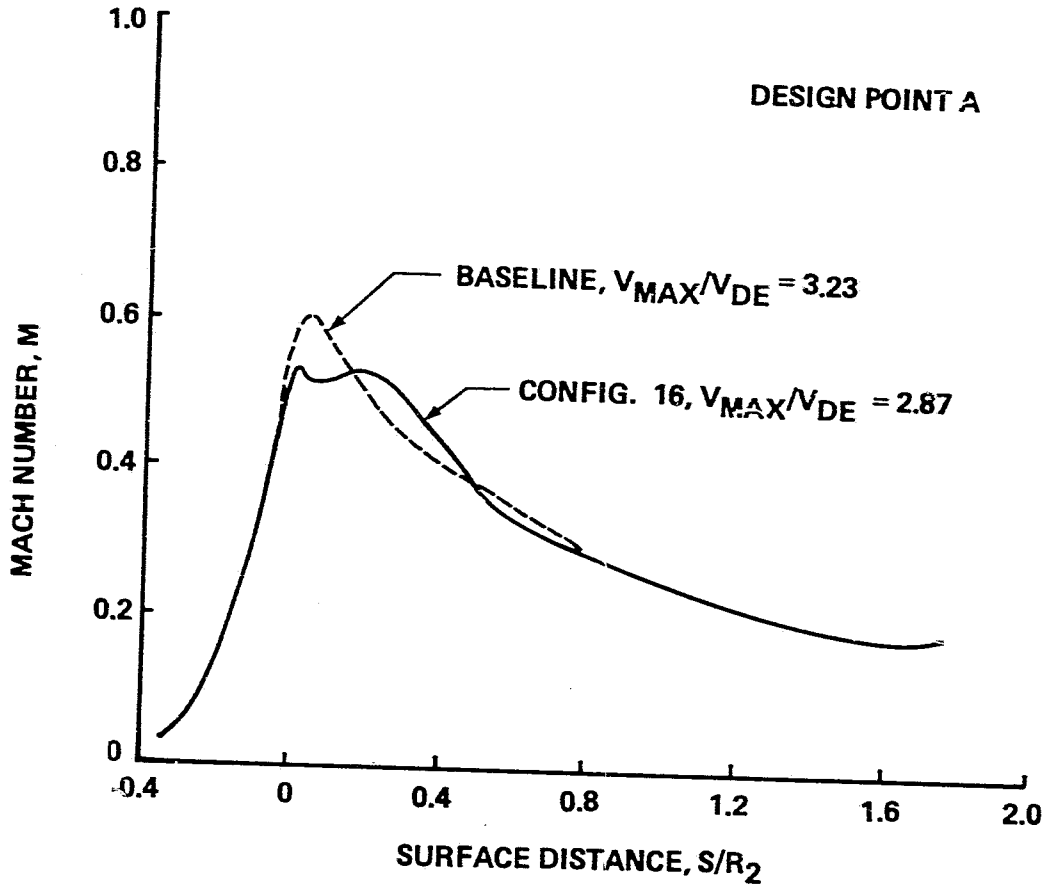

Figure 14. Mach Number Distributions for Configuration 16 and Baseline Inlet

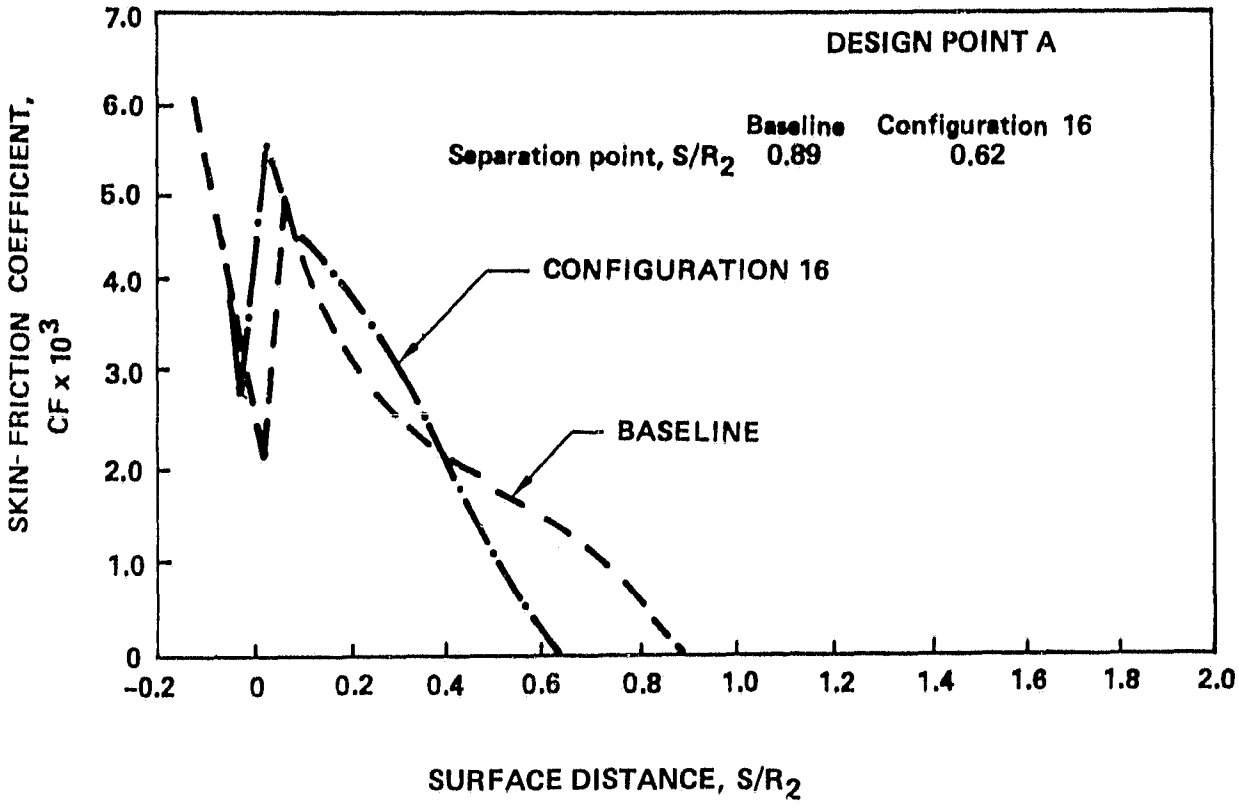

Figure 15. Skin Friction Coefficients for Configuration 16 and Baseline

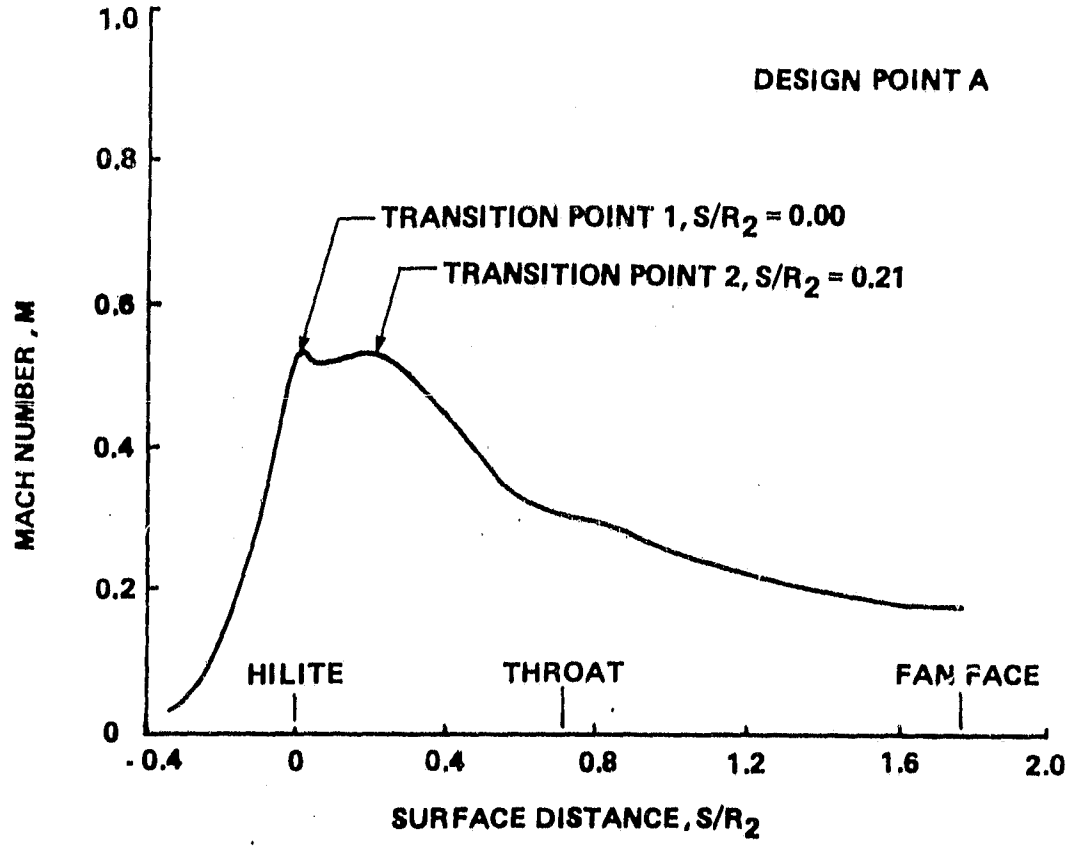

Figure 16. Transition Criteria for Configuration 16

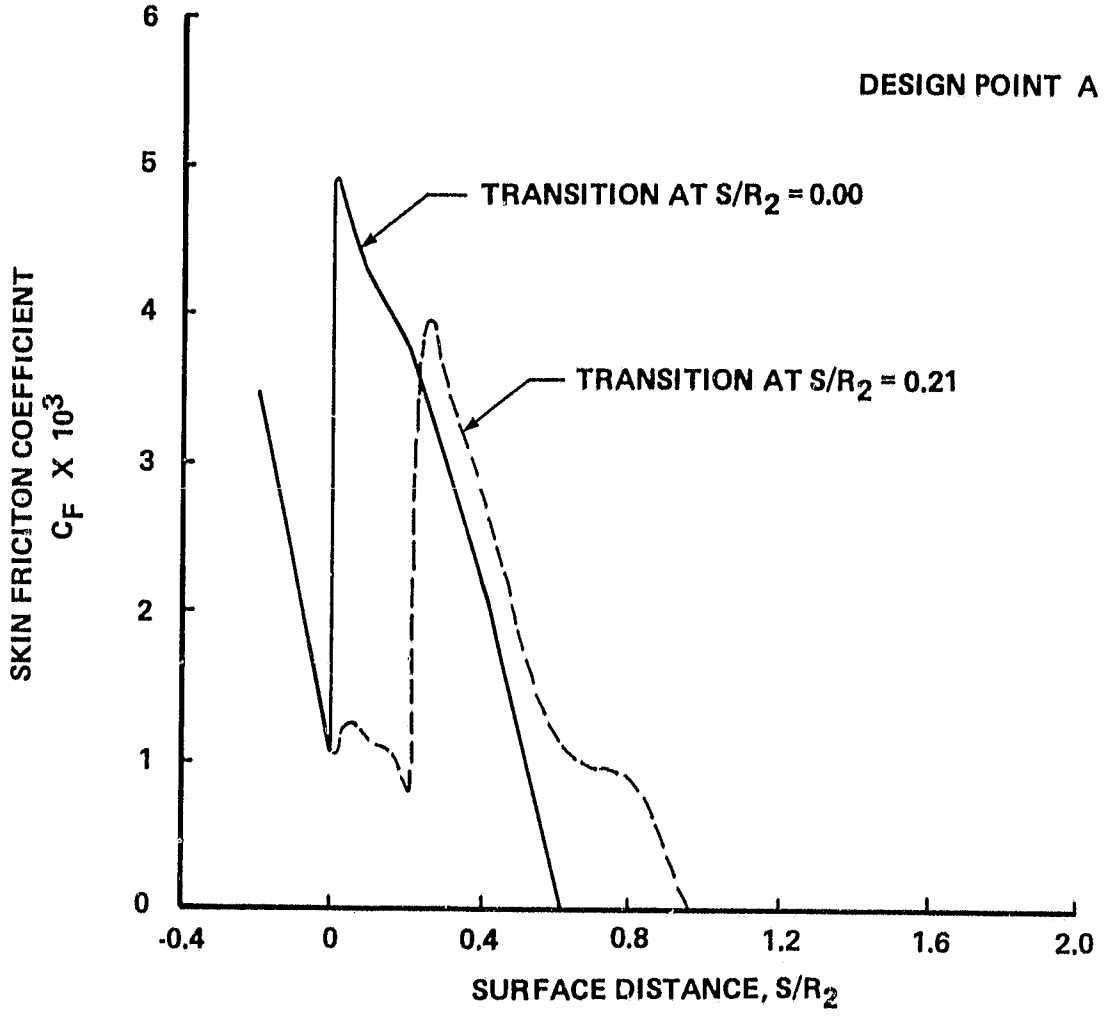

Figure 17. Effect of Transition on Separation. Configuration 16

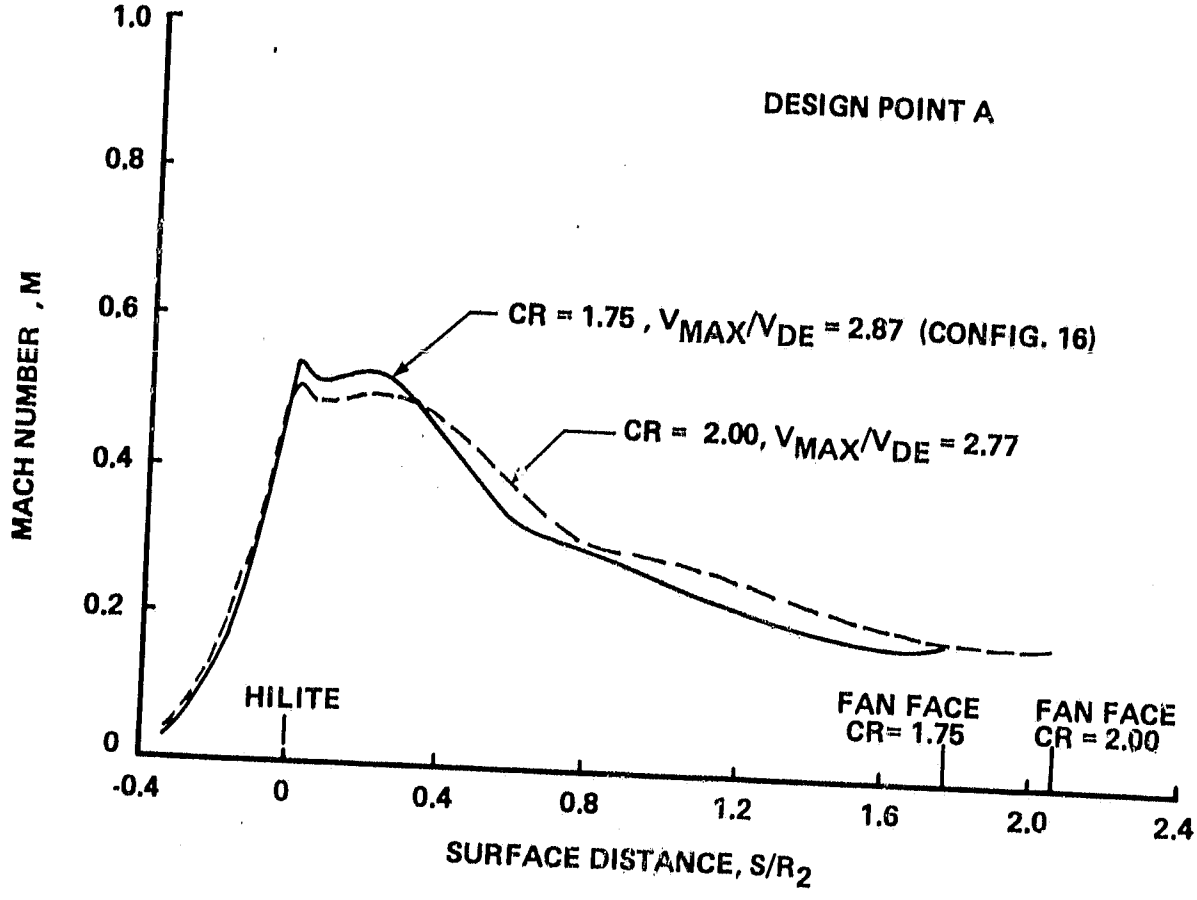

Figure 18. Effect of Contraction Ratio on Mach Number Distribution

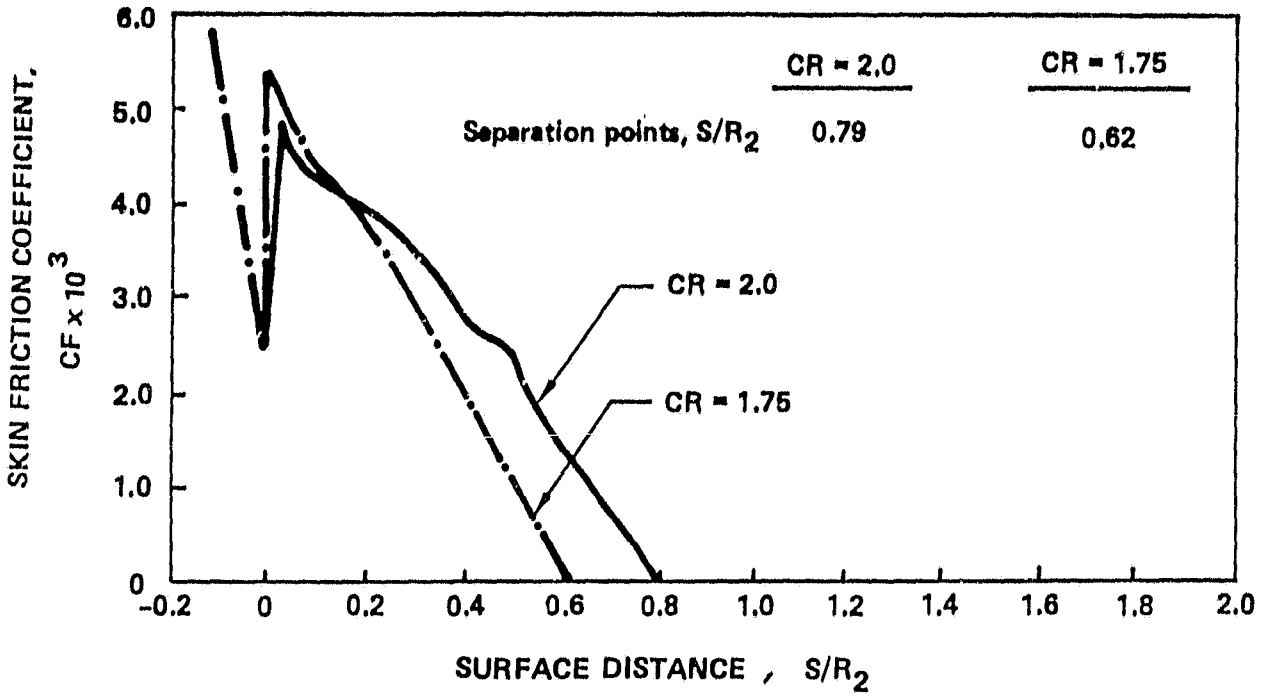

Figure 19. Effect of Contraction Ratio on Boundary Layer Development

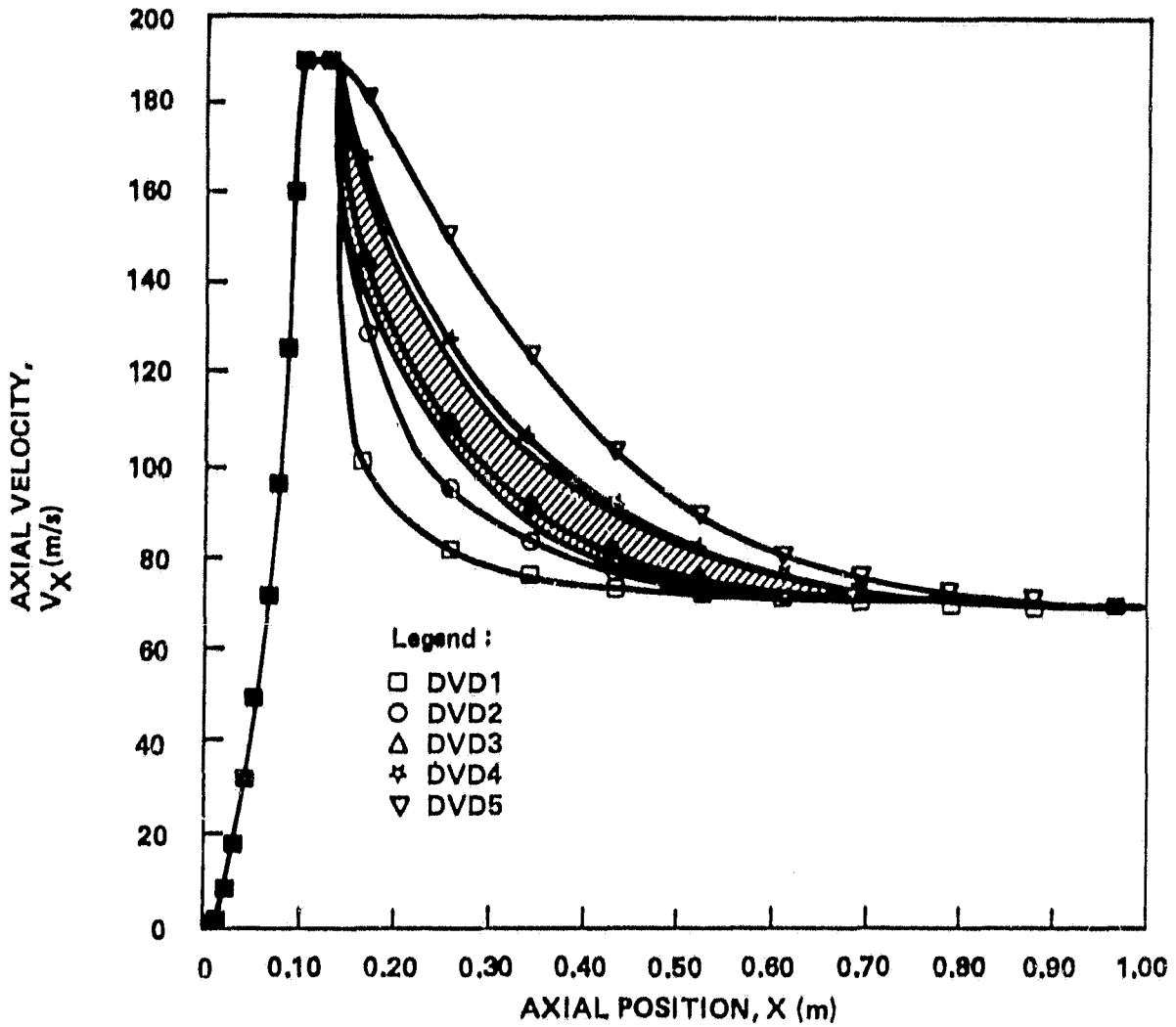

Figure 20. NASA Hypothetical Diffuser Velocity Distributions (DVD)

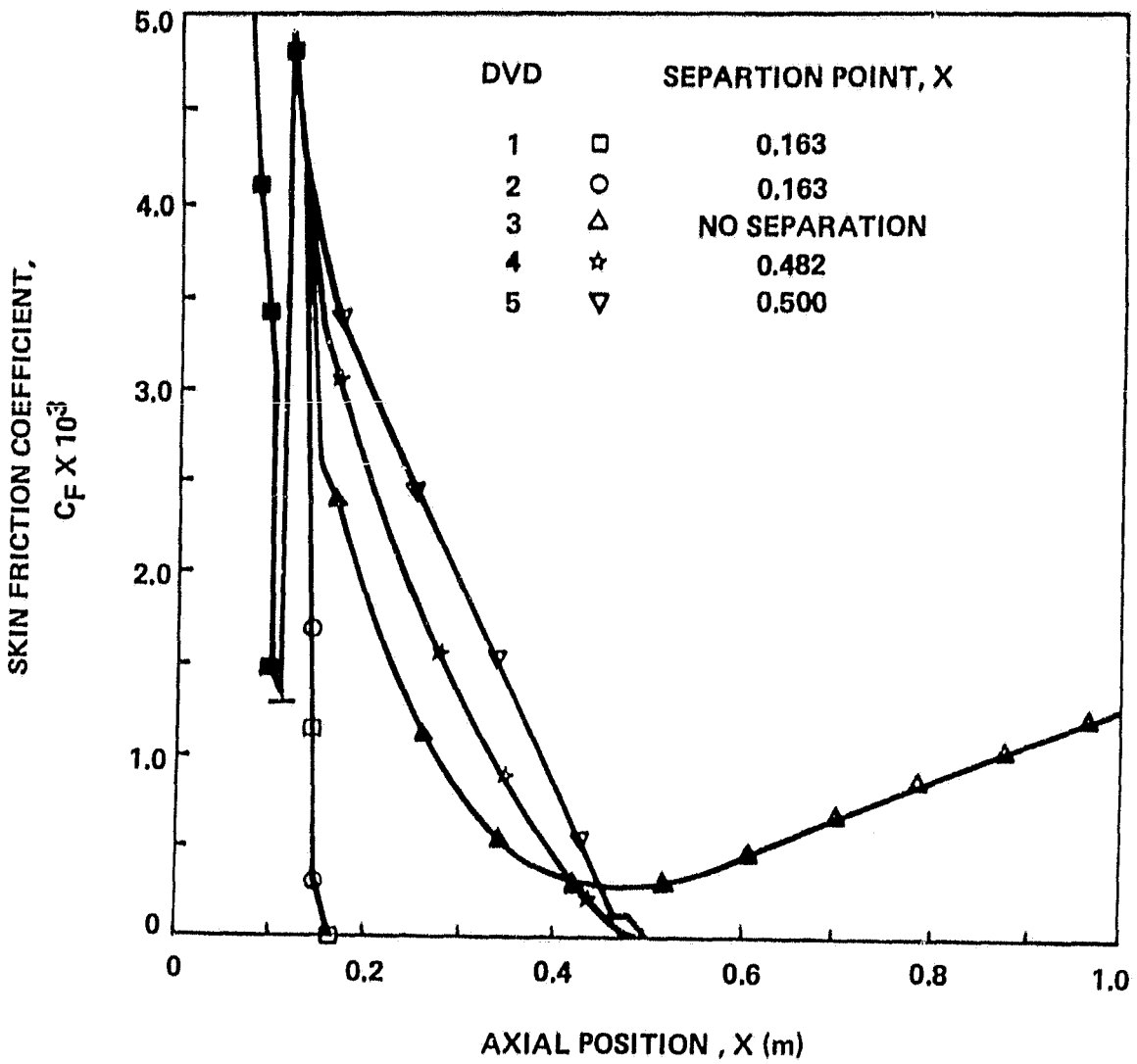

Figure 21. NASA Boundary Layer Analysis of NASA DVDs

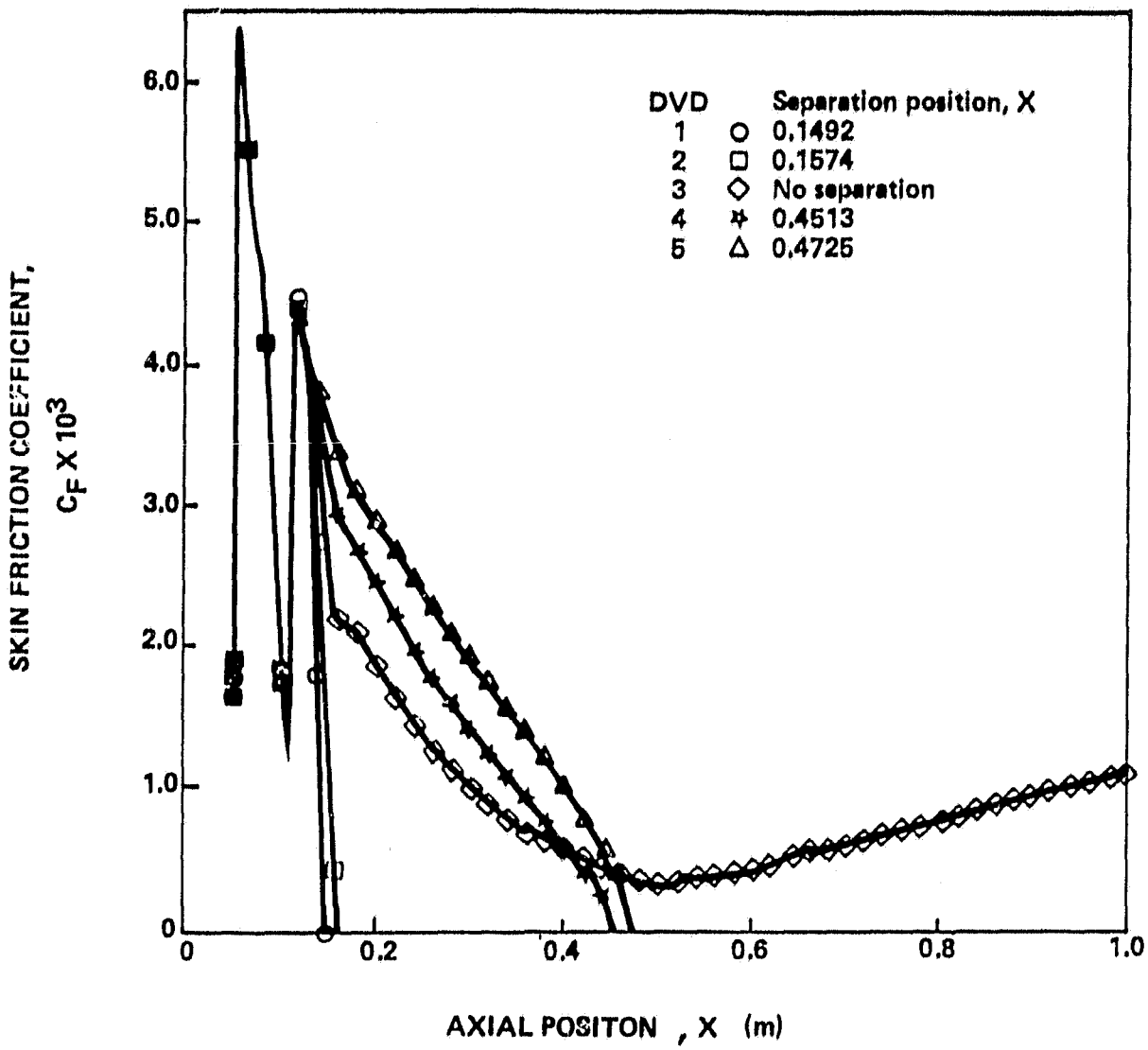

Figure 22. Boeing Boundary Layer Analysis of NASA DVDs

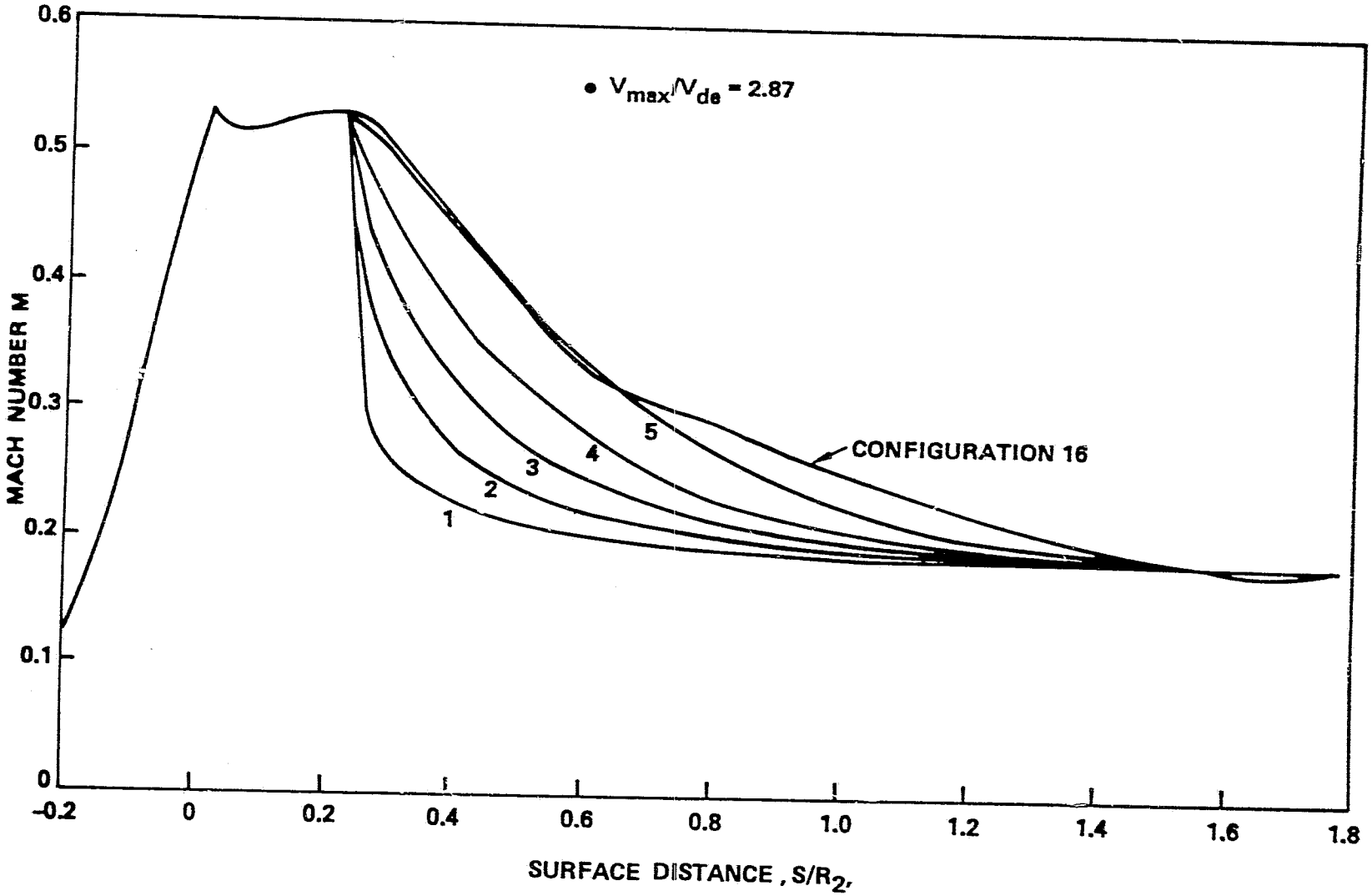

Figure 23. Parametric Diffuser Mach Number Distributions. CMD 1–5 and Configuration 16

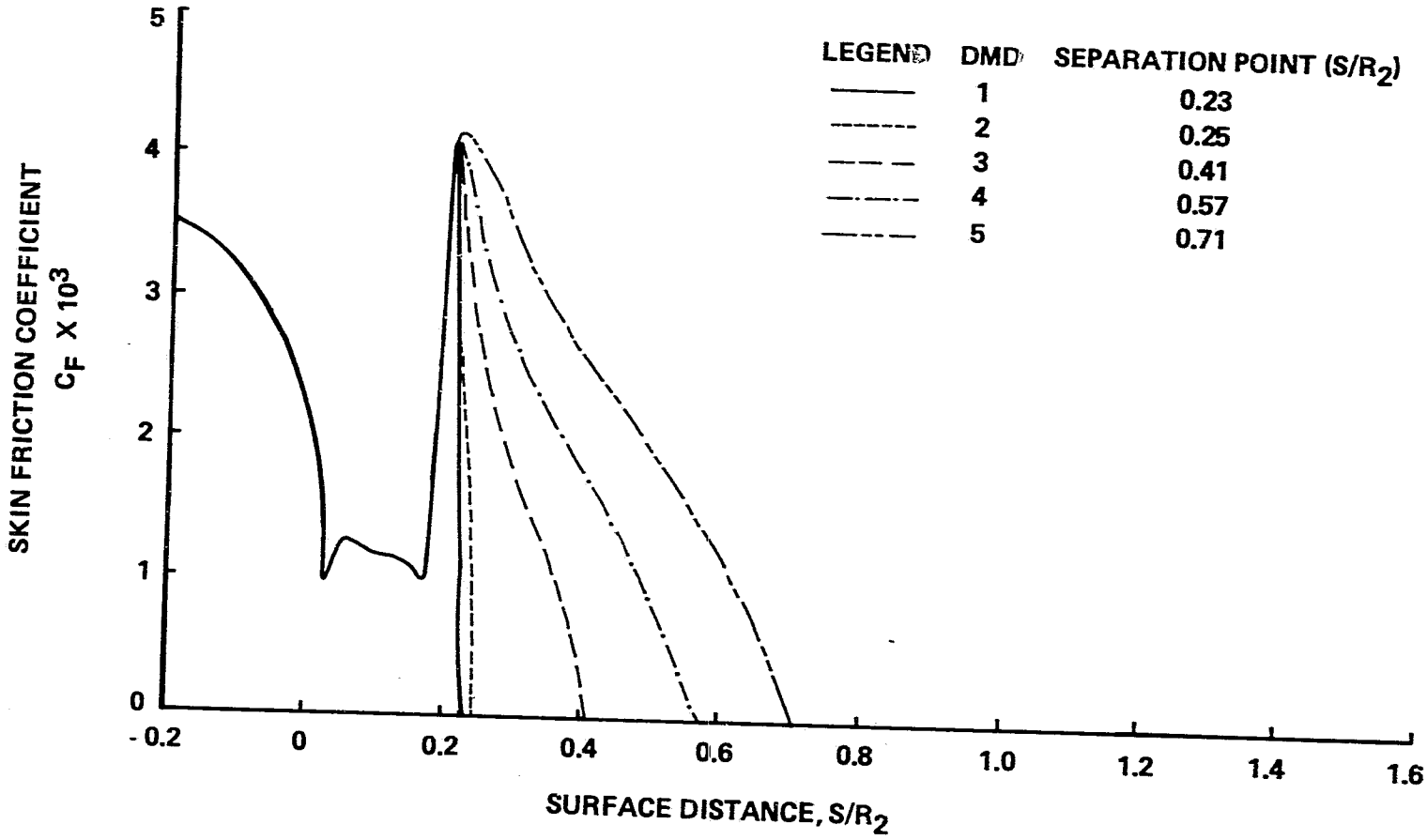

Figure 24. Boundary Layer Analysis of DMD 1–5

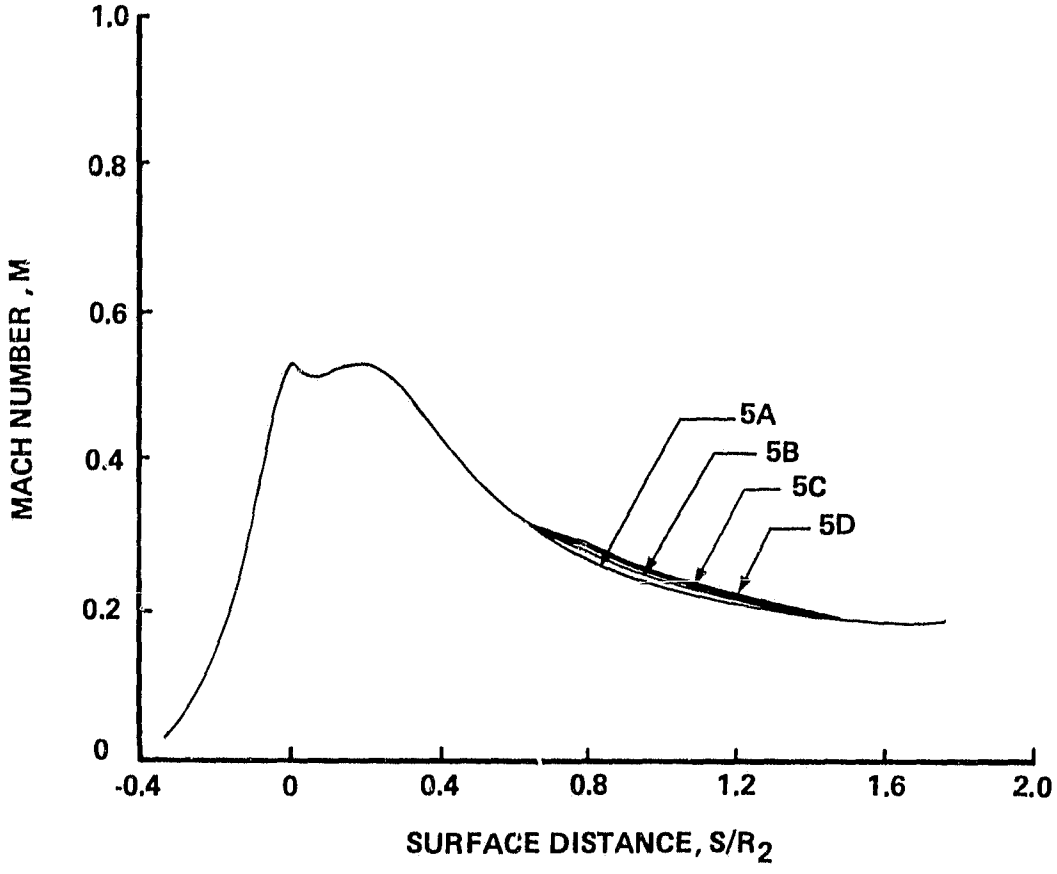

Figure 25. Hypothetical Mach Number Distributions between DMD 5 and Configuration 16. DMD 5A, 5B, 5C, 5D

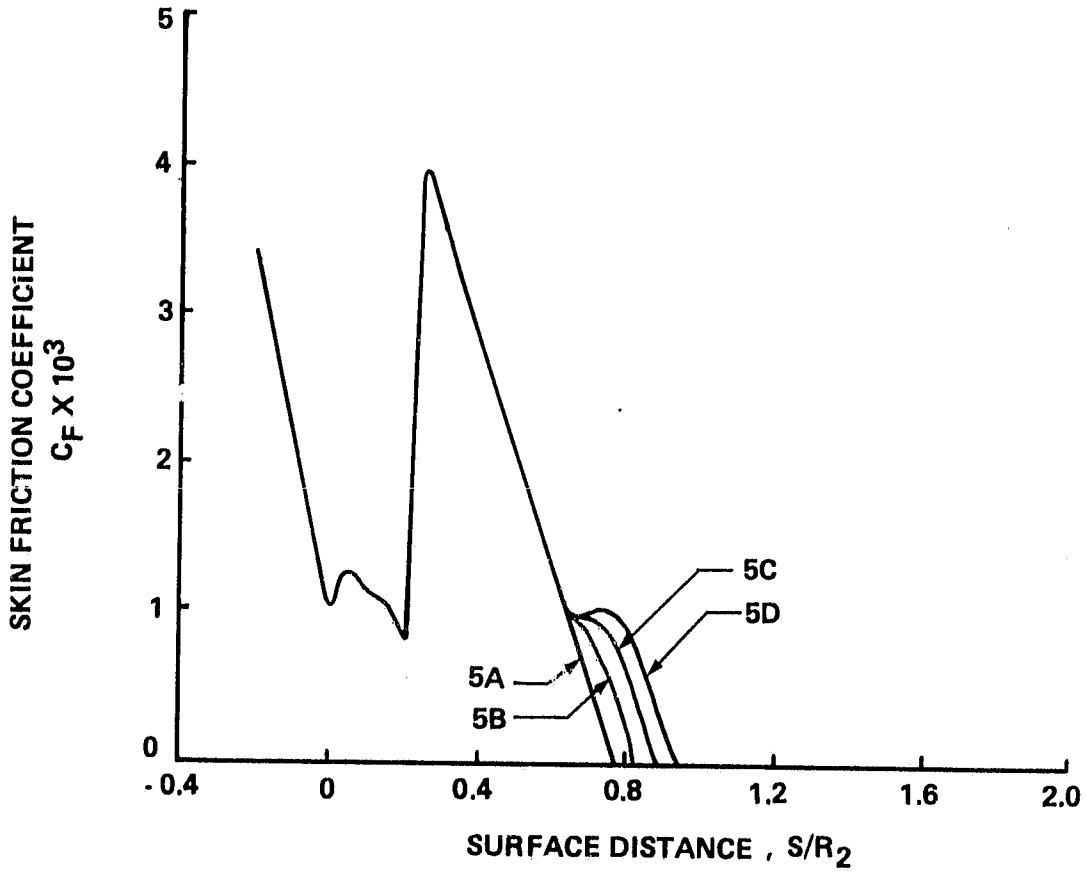

Figure 26. Boundary Layer Analysis of DMD 5A, 5B, 5C, 5D

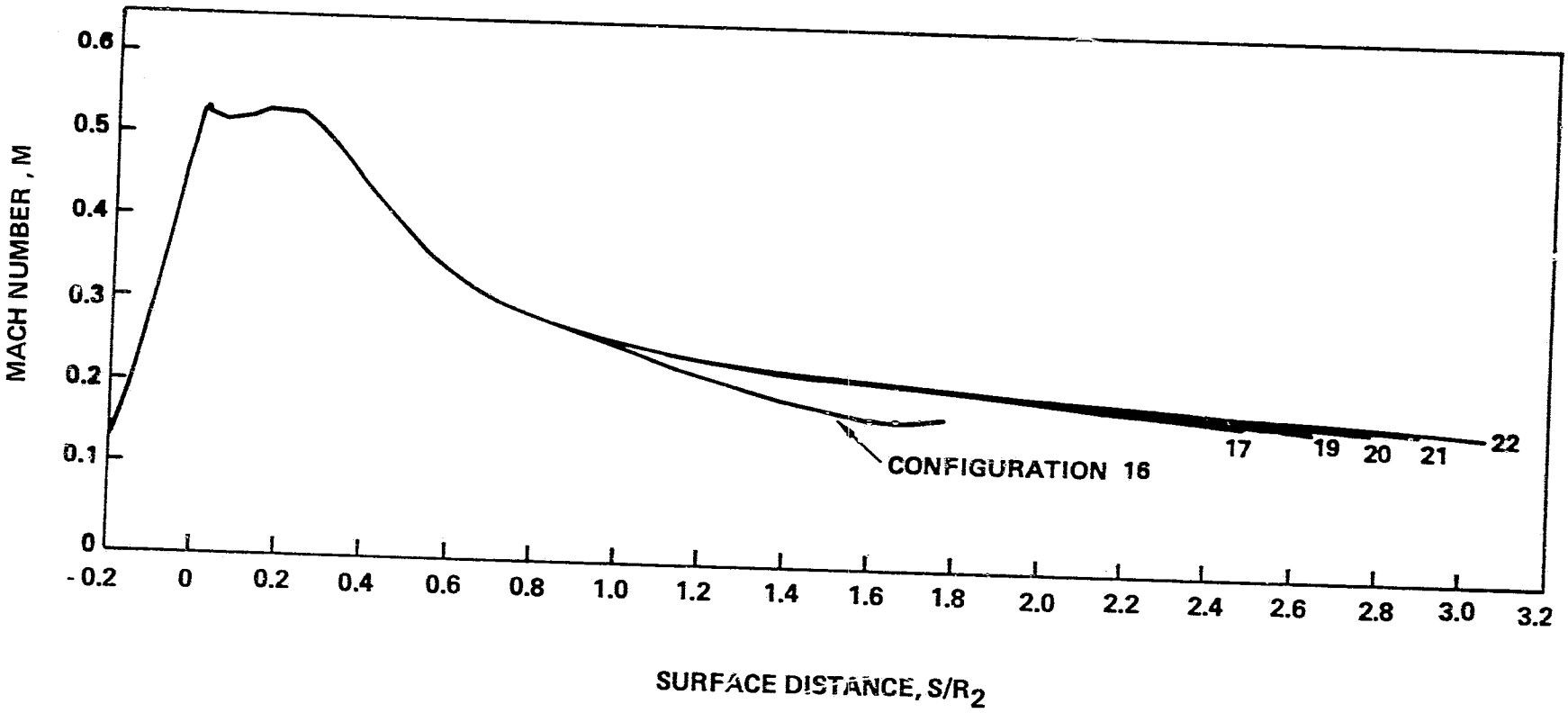

Figure 27. Diffuser Mach Number Distributions. Configuration 16 and DMD 17–22

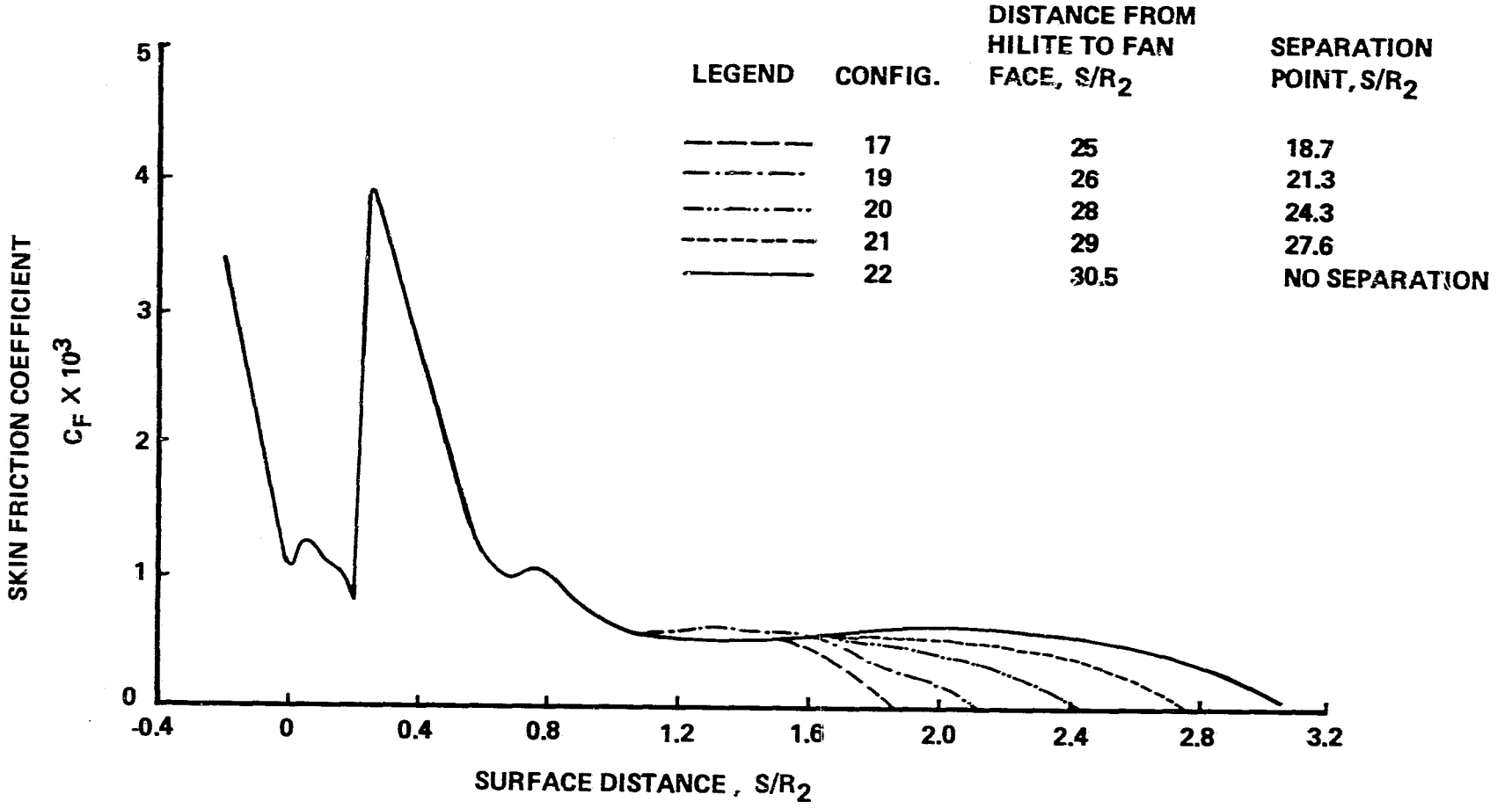

Figure 28. Boundary Layer Analysis of DMD 17–22

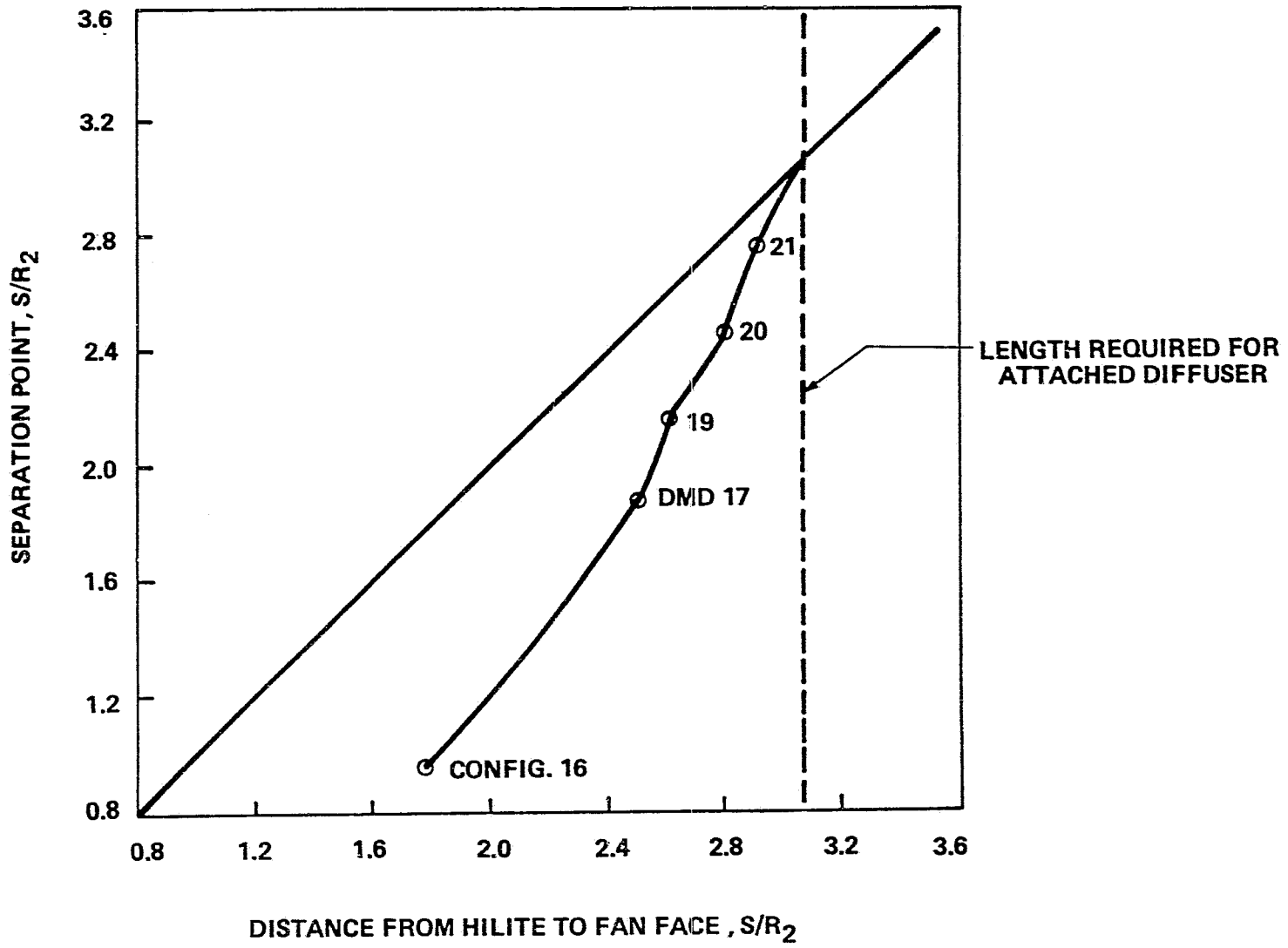

Figure 29. Separation Point as a Function of Diffuser Length

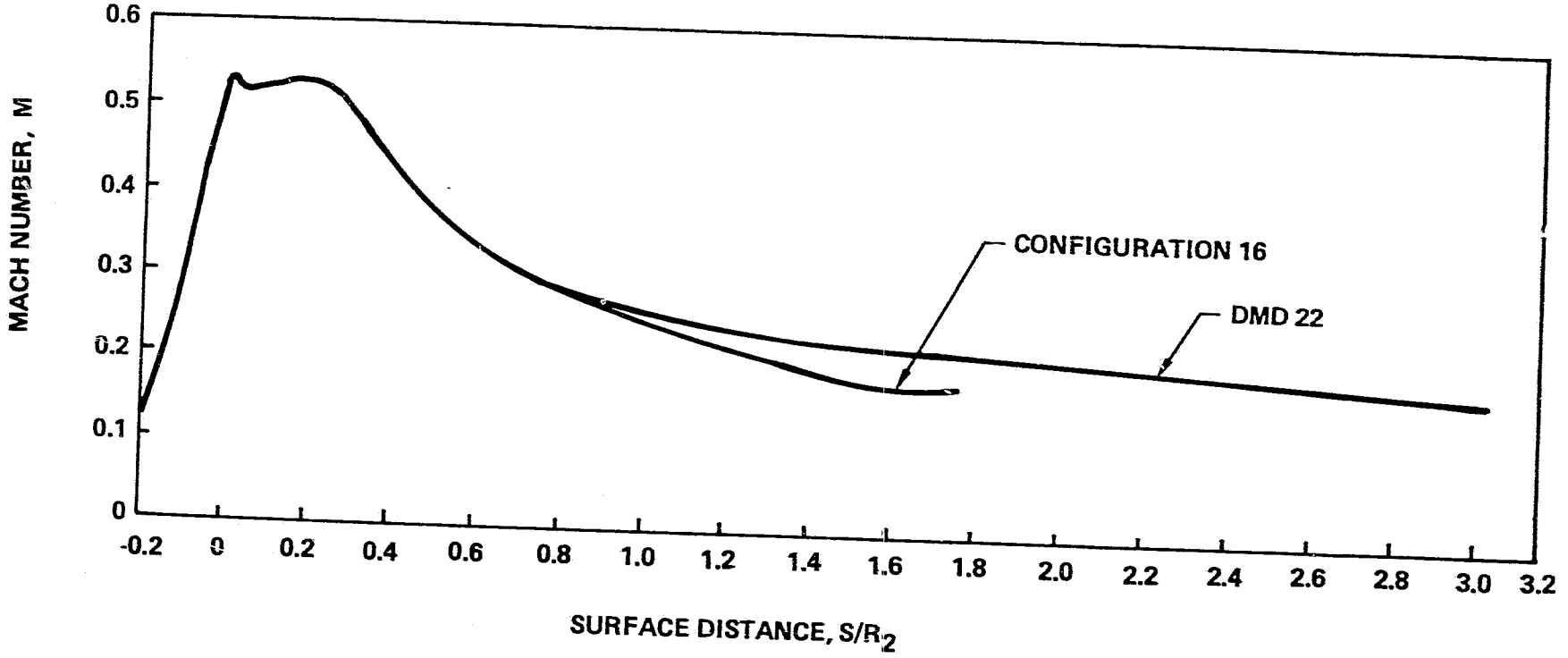

Figure 30. Diffuser Mach Number Distributions. DMD 22 and Configuration 16

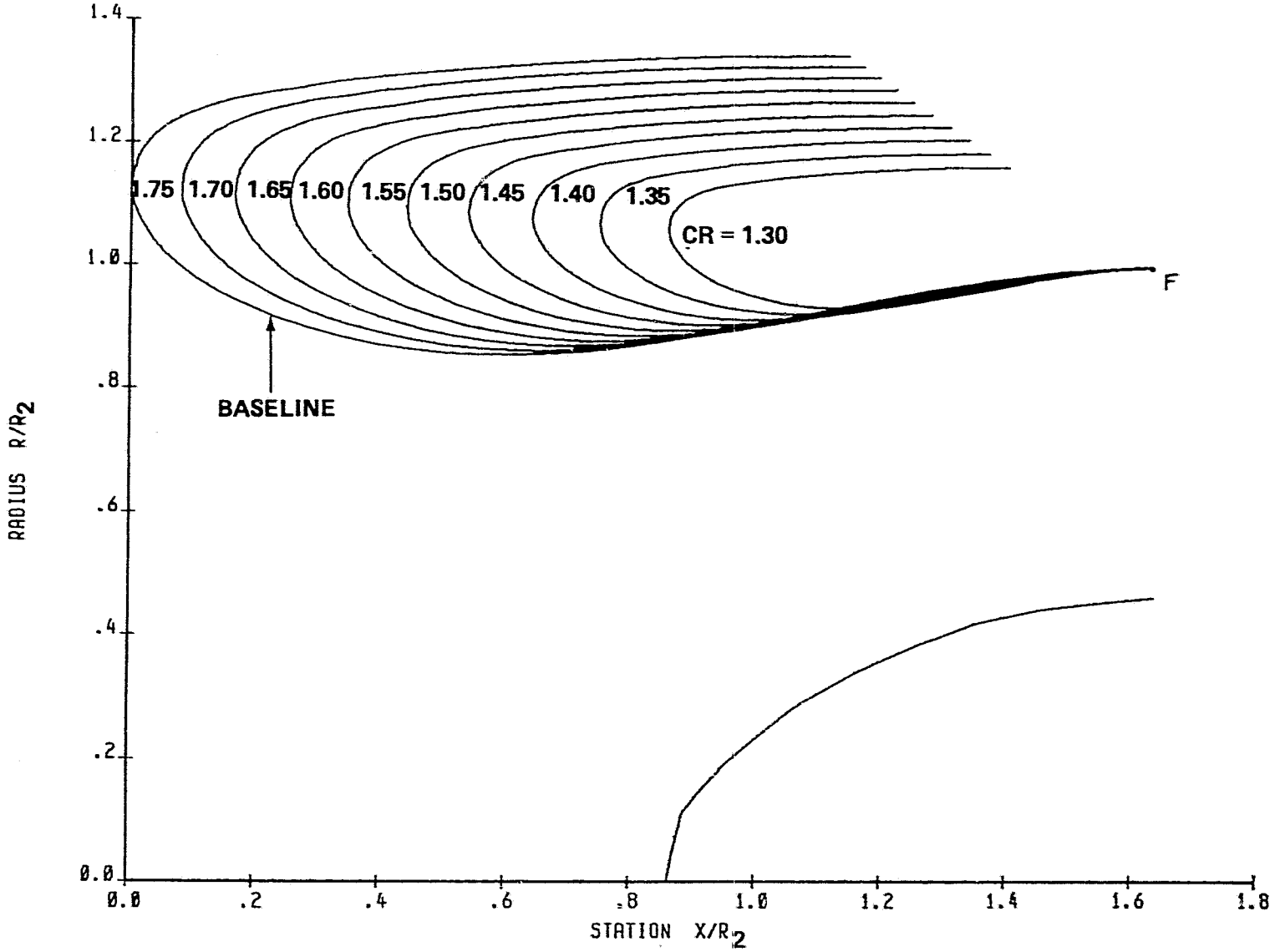

Figure 31. Baseline and Reduced CR Inlets. Contraction Ratios 1.30–1.75

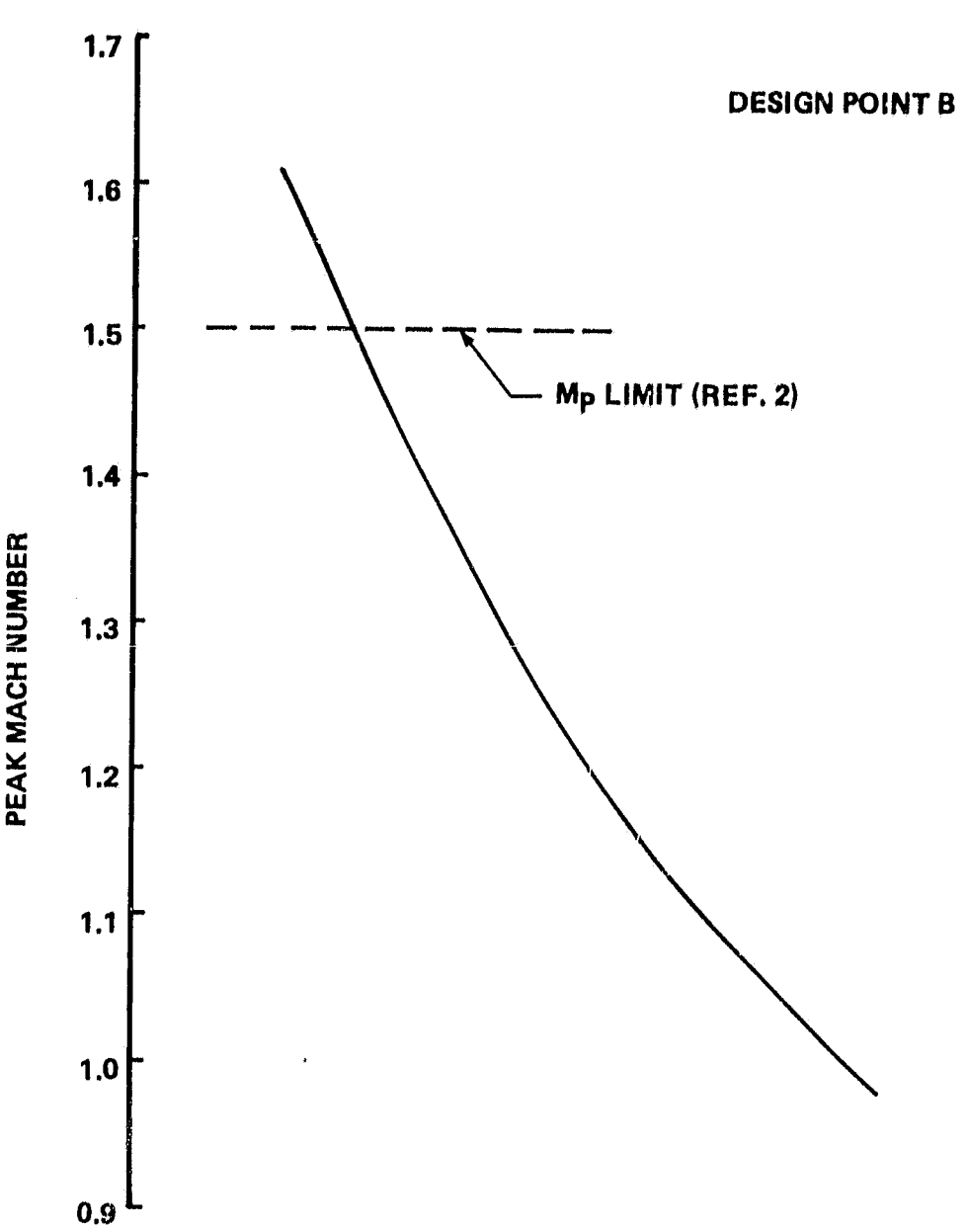

Figure 32. Peak Mach Numbers at Conditon B for Baseline and Reduced CR Inlets

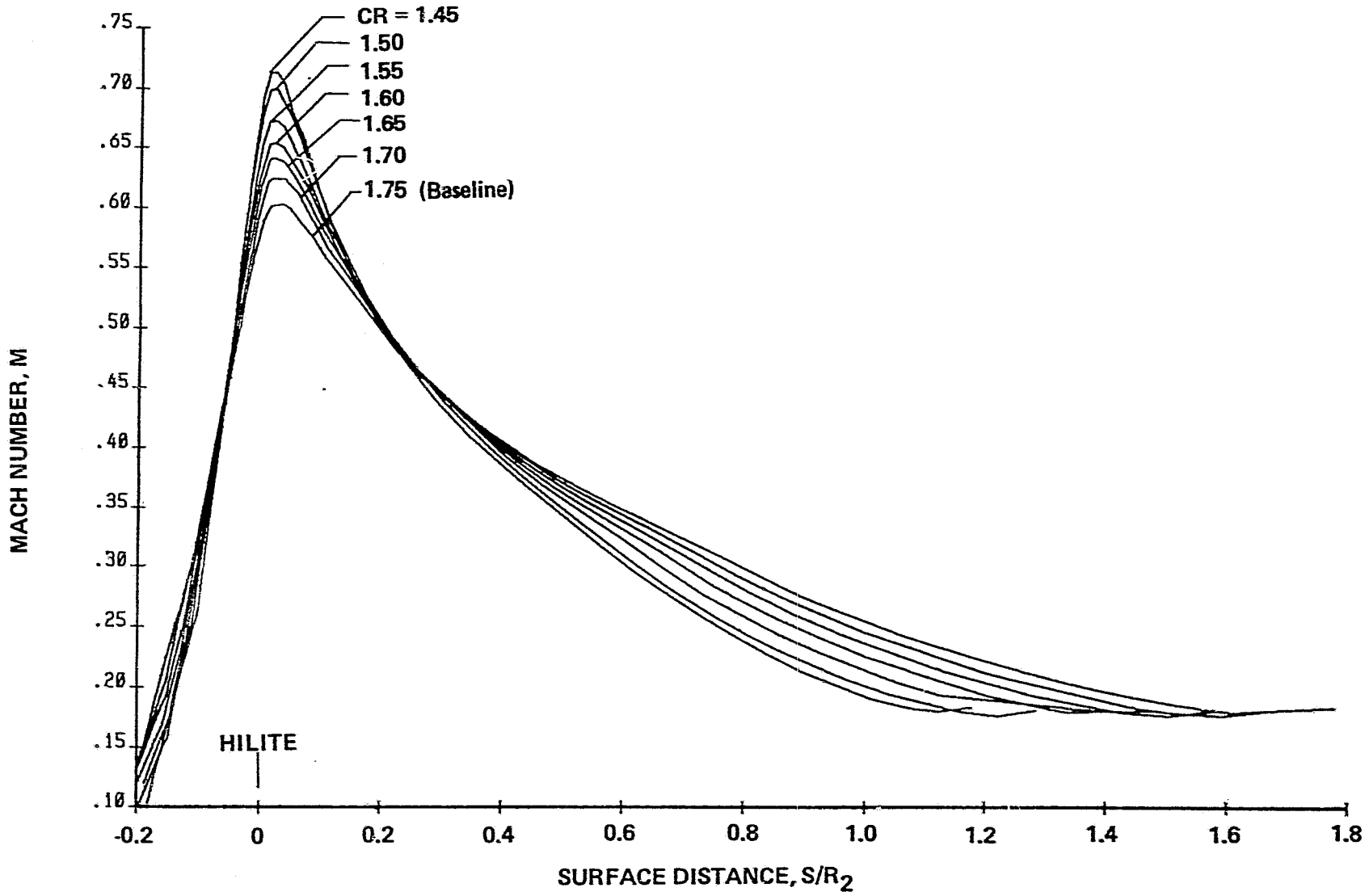

Figure 33. Mach Number Distributions at Condition A for Baseline and Reduced CR Inlets

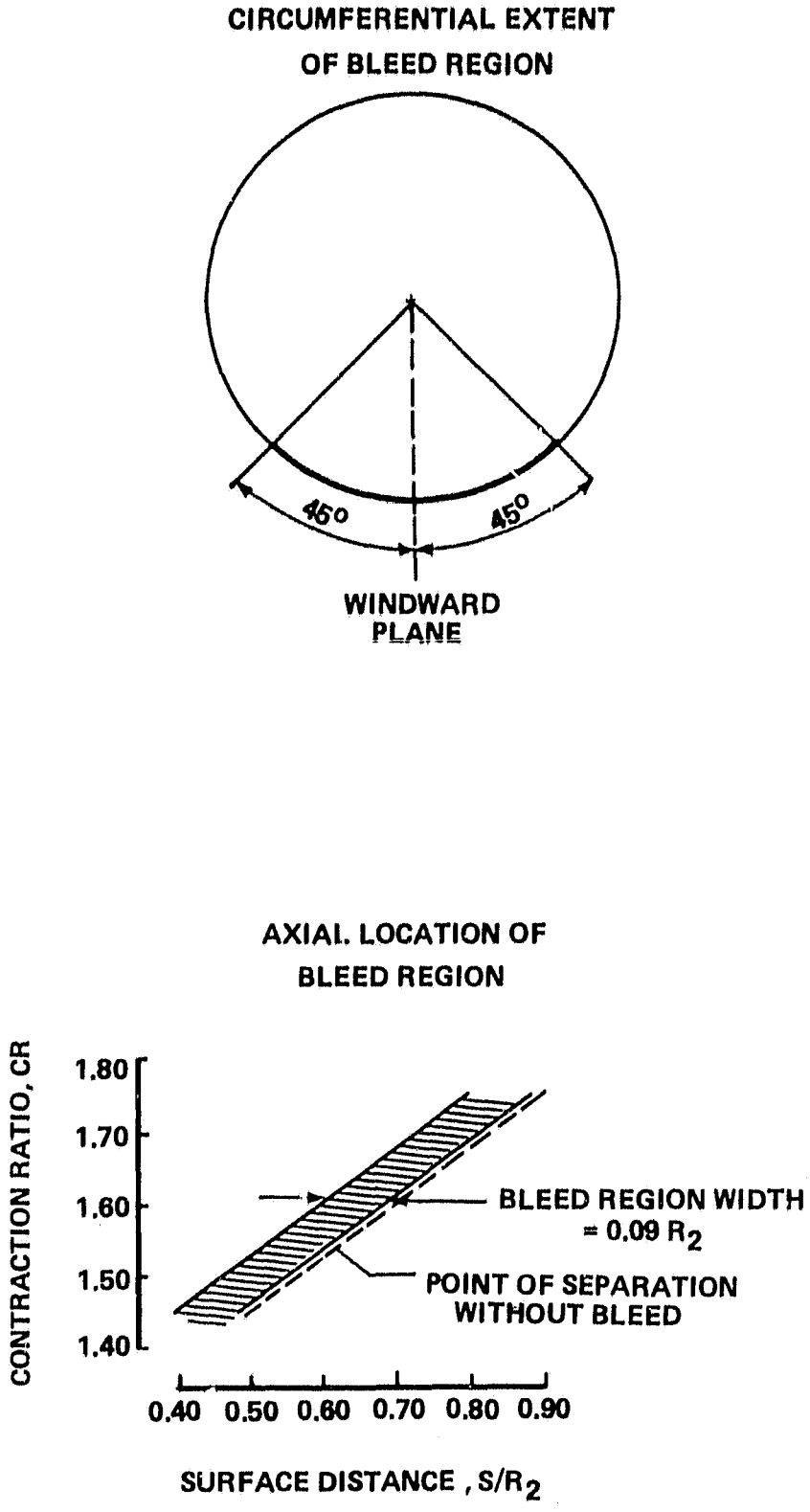

Figure 34. Locations and Dimensions of Bleed Regions

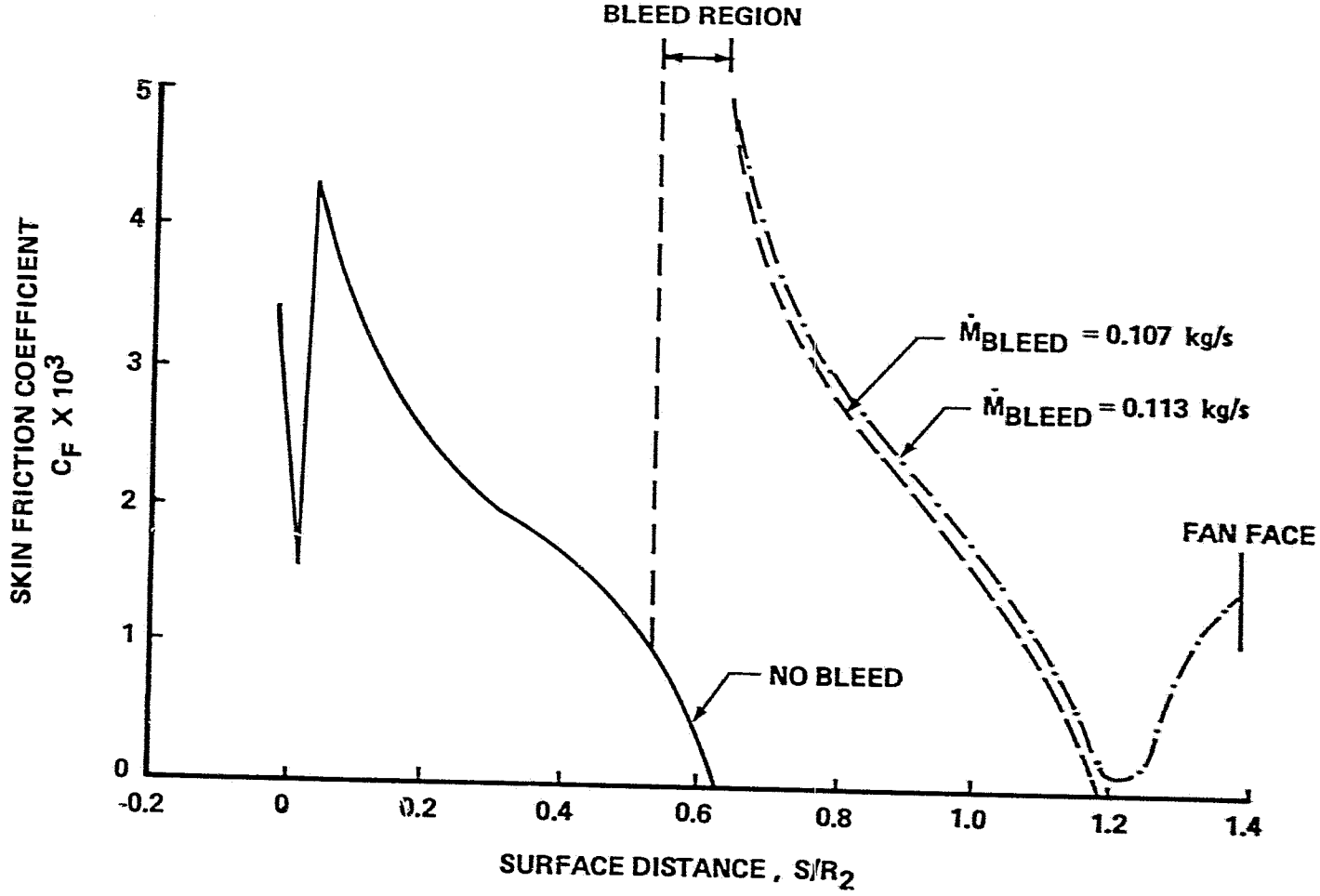

Figure 35. Boundary Layer Analysis for CR = 1.55 Inlet With and Without Bleed

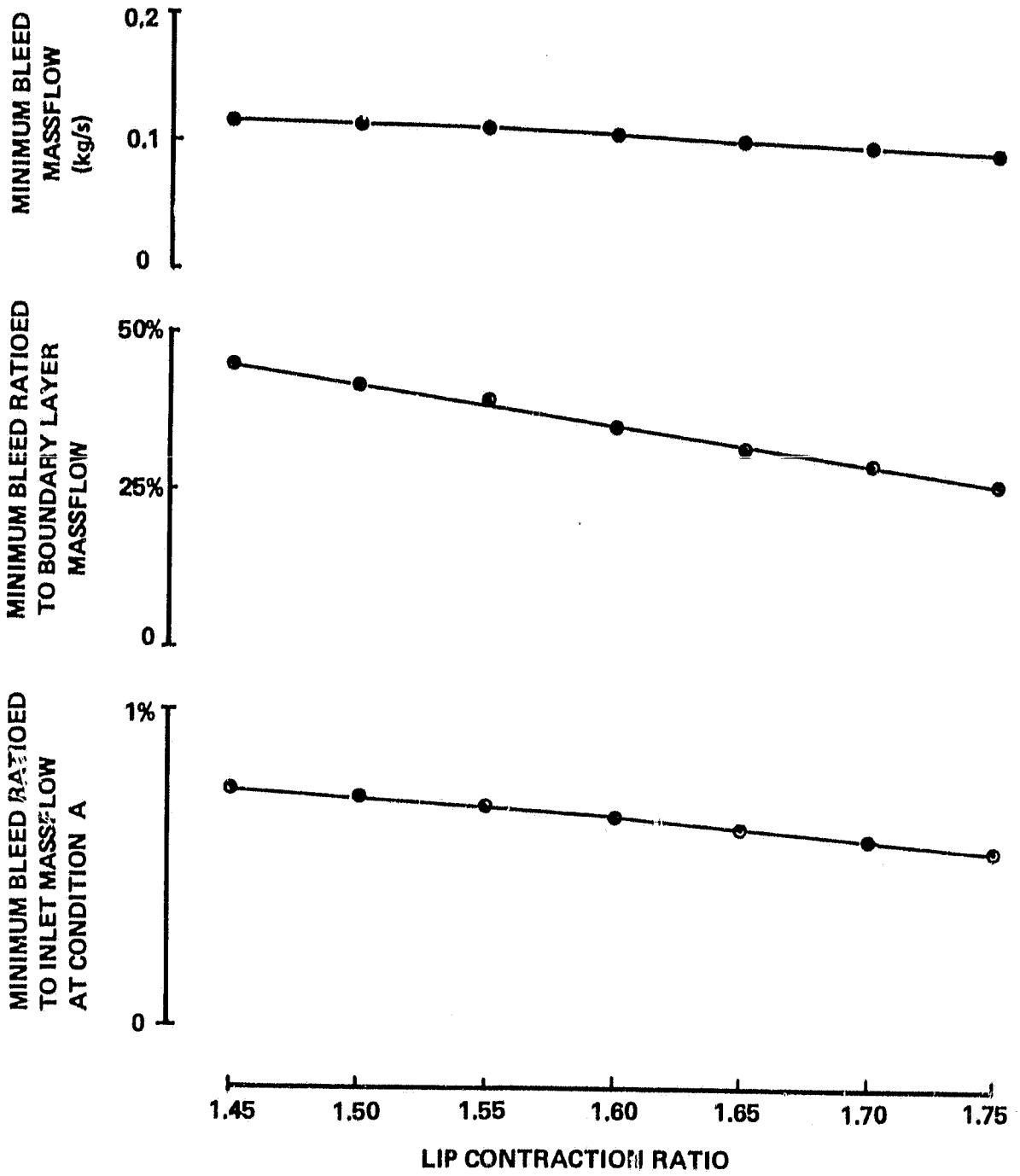

Figure 36. Minimum Bleed for Attached Flow at Design Point A

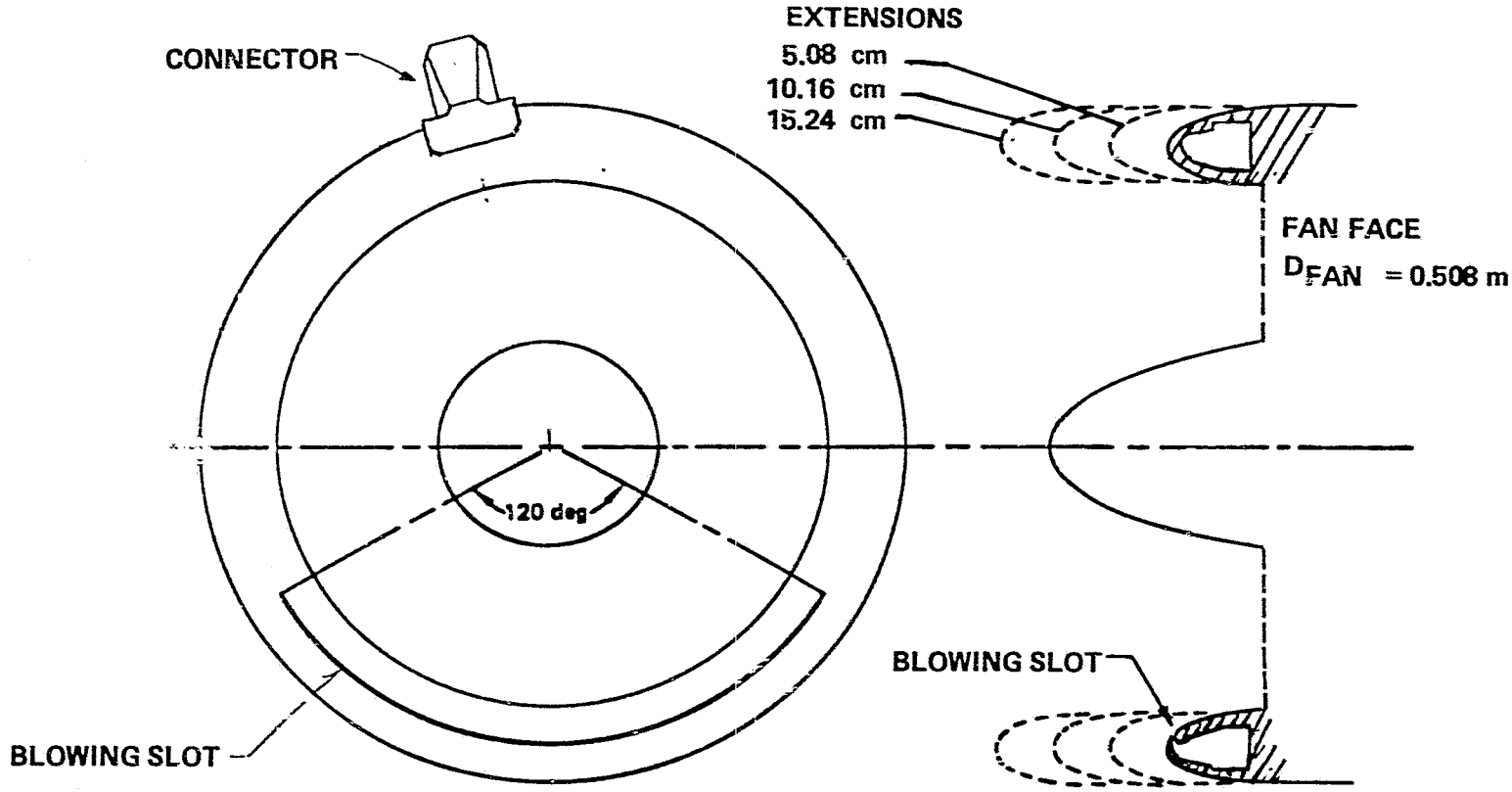

Figure 37. Schematic of Blowing-Lip Inlet Model

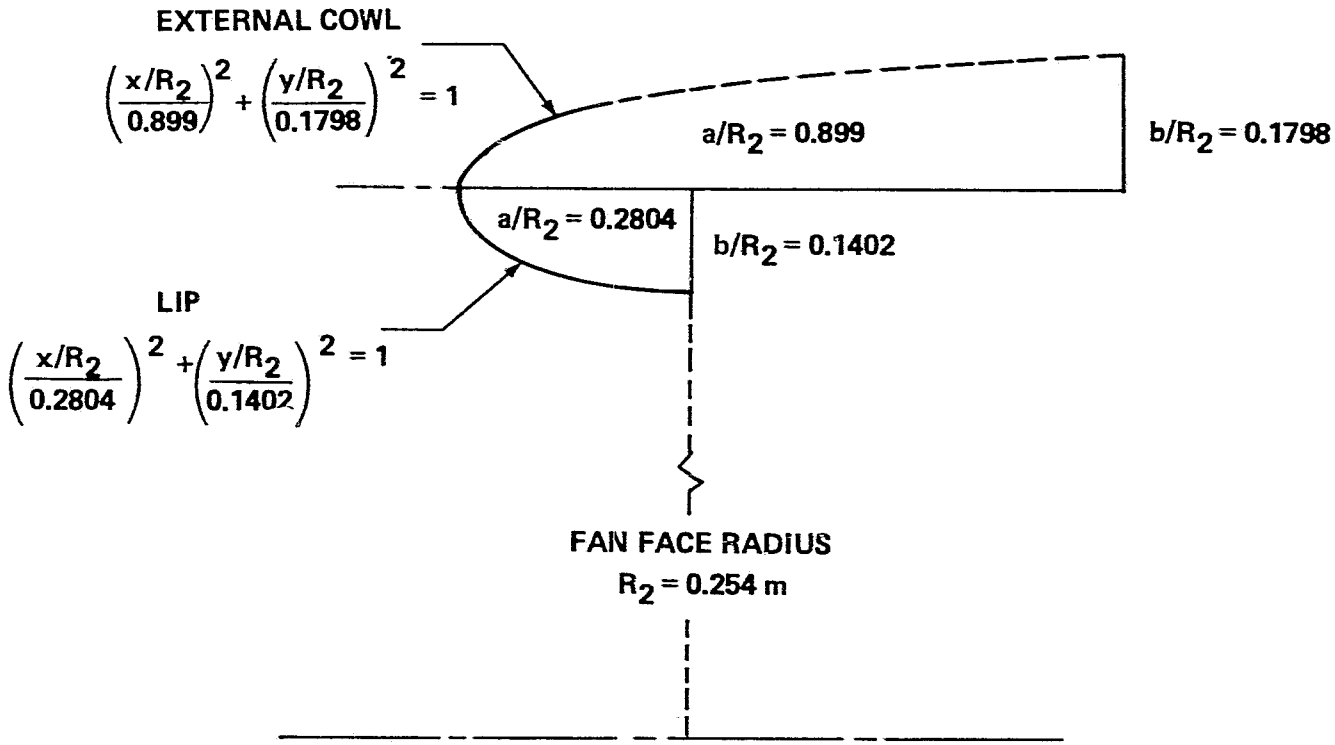

Figure 38. Lip and External Cowl Contours

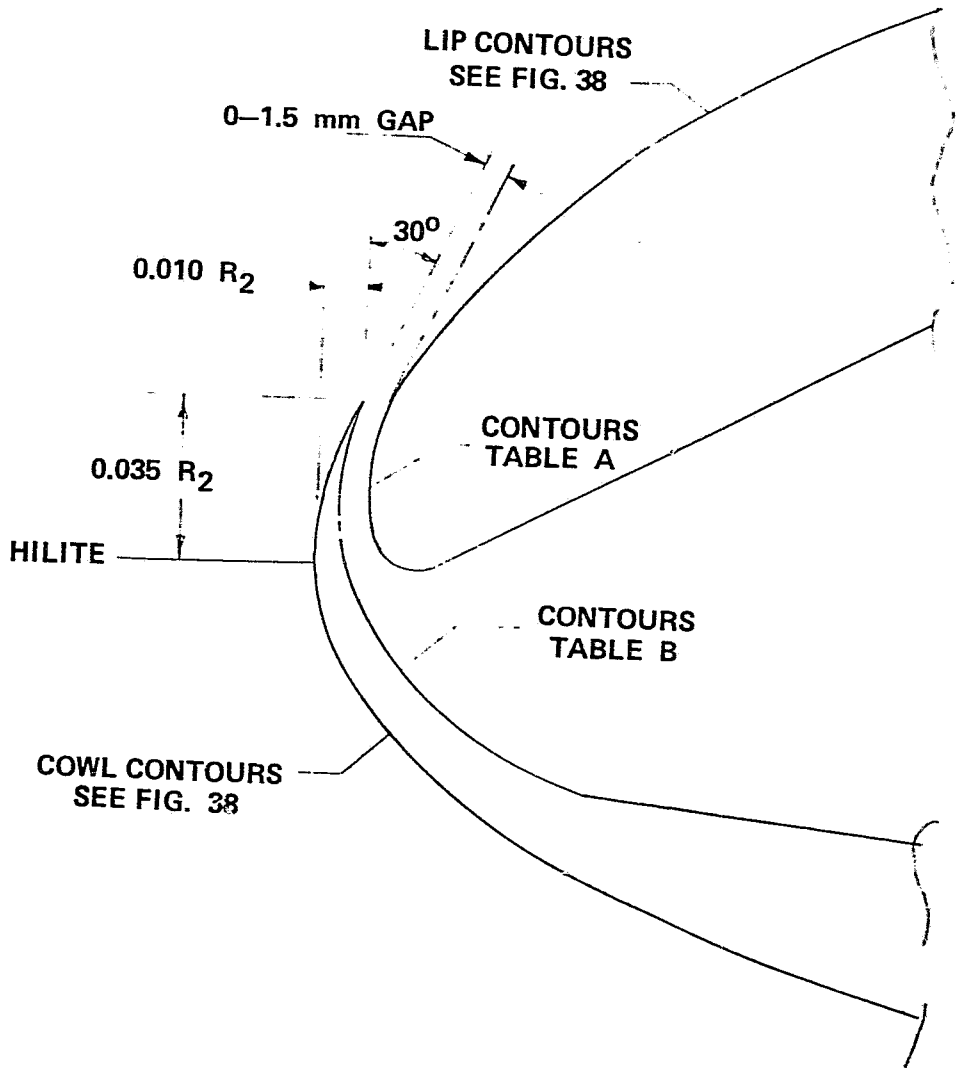

Figure 39. Slot Geometry Details

TABLE A

X/R_2	R/R_2
.0172	1.1402
.0150	1.1395
.0100	1.1331
.0077	1.1282
.0073	1.1236
.0077	1.1182
.0100	1.1095
.0150	1.0978
.0172	1.0934
.0200	1.0895
.0300	1.0771
.0400	1.0680
.0500	1.0603

TABLE B

X/R_2	R/R_2
0.0100	1.1050
0.0096	1.1096
0.0073	1.1122
0.0056	1.1306
0.0070	1.1418
0.0090	1.1470
0.0100	1.1508
0.0125	1.1540
0.0150	1.1591
0.0200	1.1654
0.0300	1.1734
0.0400	1.1782
0.0500	1.1804

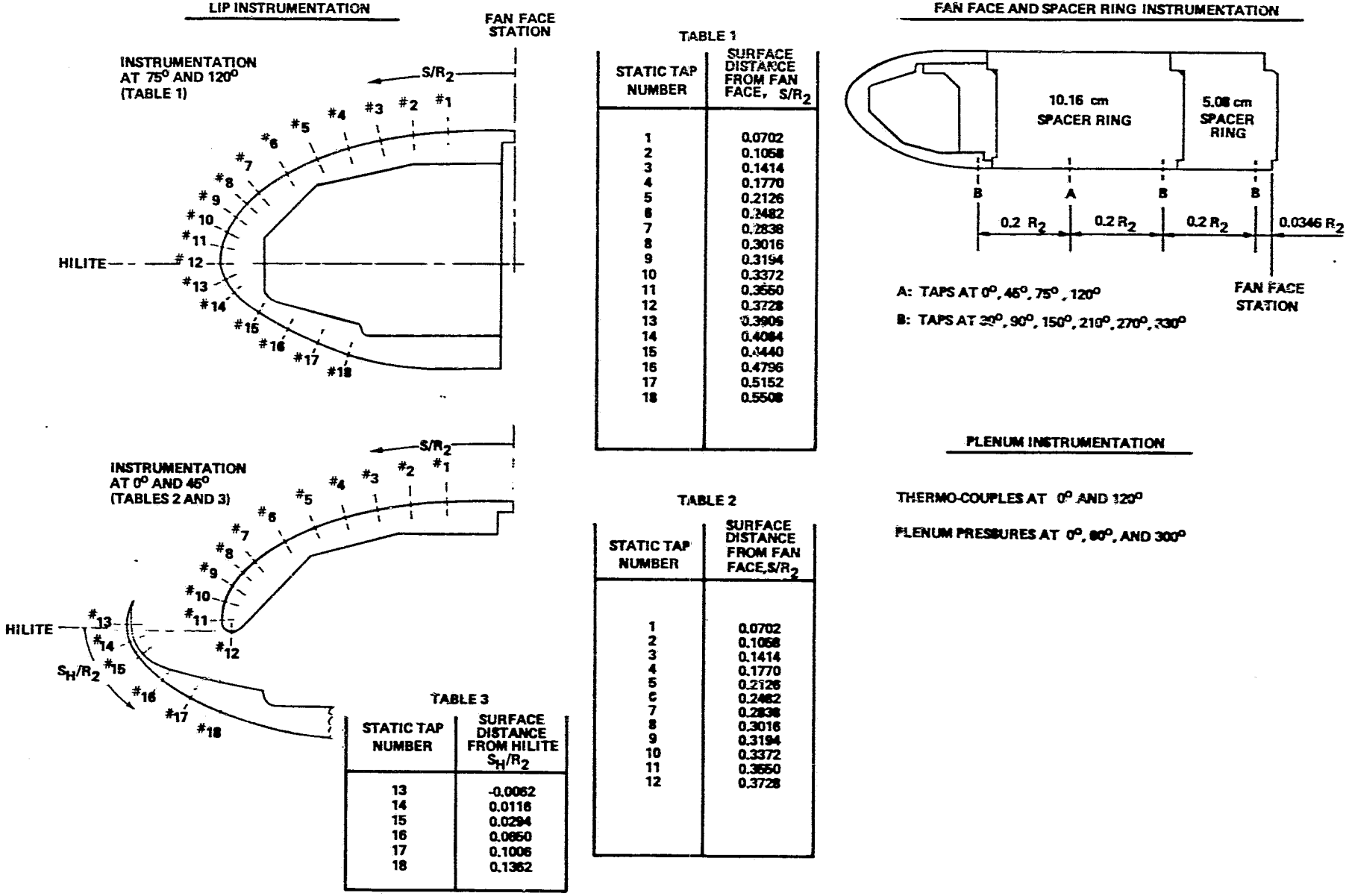

TABLE 1

STATIC TAP NUMBER	SURFACE DISTANCE FROM FAN FACE, S/R_2
1	0.0702
2	0.1058
3	0.1414
4	0.1770
5	0.2126
6	0.2482
7	0.2838
8	0.3016
9	0.3194
10	0.3372
11	0.3550
12	0.3728
13	0.3906
14	0.4084
15	0.4440
16	0.4796
17	0.5152
18	0.5508

TABLE 2

STATIC TAP NUMBER	SURFACE DISTANCE FROM FAN FACE, S/R_2
1	0.0702
2	0.1058
3	0.1414
4	0.1770
5	0.2126
6	0.2482
7	0.2838
8	0.3016
9	0.3194
10	0.3372
11	0.3550
12	0.3728

TABLE 3

STATIC TAP NUMBER	SURFACE DISTANCE FROM HILITE S_H/R_2
13	-0.0062
14	0.0116
15	0.0294
16	0.0650
17	0.1006
18	0.1362

Figure 40. Instrumentation Details